



# Investigation on influence of oil on composite materials

Jaykishan Patel (MSc. Automotive Engineering)

Czech Technical University in Prague

## Supervisor

Ing. Lukáš Kazda

**Declaration**

I hereby declare that this diploma thesis project has been written by me in person. All the information used from other scholar's work has been acknowledged in the text with the list of references presented in the bibliography section.

In Prague: 13.08.2021



---

**Jaykishan Patel**

## Abstract

The application of composite materials in the automotive industry have become prominent in the recent years due to make the industry more sustainable and cost efficient, without compromising the performance of automobiles. Uses of fiber reinforced polymer composite (FRPs) material in an automobile are not only limited to structural parts, but it can also have its application in powertrain components, interiors, suspension parts, brakes, and fuel pumps. Therefore, it is extremely crucial to meticulously understand the service life, degradation behavior and failure modes of FRP composite parts used in cars. This paper will study the application of FRP material in automotive field, and the effect of oil on the performance of composite material parts.

**Keywords:** CFRP composite, oil, Automotive, Matlab, Abaqus, FEM Analysis, Diffusion, tensile test, Elastic behavior

# Acknowledgments

Firstly, I would like to thank my professor and mentor Ing. Lukas Kazda for giving me this opportunity. His guidance, constant support, and knowledge of the subject motivated me throughout the period of the diploma project and helped to accomplish the project goals. In addition, I would like to thank the head of the Advanced Powertrains and transmission department Doc. Dr. Ing. Gabriela Achtenova for approving the thesis topic, and to Czech University of Life Science Prague, Faculty of Engineering for providing the permission to the resources and conduct experiments on their facility. Lastly, I would like to thank my family and friends for their endless support in any way and form.

**Jaykishan Patel**

# Table of Contents

Abstract .....	3
1 Introduction.....	10
1.1 Background.....	10
1.2 Objective .....	11
1.2.1 Research question: .....	11
2 Literature Review.....	12
2.1 Influence of working fluid on composite materials.....	12
2.2 Modelling .....	18
3 Specimen used and Experimental Methodology.....	19
3.1 Specimen Material.....	19
3.2 Specimen Shape and Dimension .....	21
3.3 Experimental Methodology .....	22
3.3.1 Conditioning the 3D printed composite samples.....	22
3.3.2 Tensile testing.....	23
4 Programs and Mathematical equations.....	25
4.1 Diadem-NI and Excel.....	25
4.2 Matlab.....	28
4.2.1 Mathematical equations used for the Diffusion analysis .....	29
4.2.2 Calculations of diffusion parameters $D_{11}$ , $D_{22}$ , $D_{33}$ .....	31
4.2.3 Moisture uptake and Moisture Saturation Content.....	31
4.3 Abaqus .....	32
4.3.1 Governing equation in Abaqus CAE for Diffusion model.....	32

Thesis Report	6
5 Analysis.....	34
5.1 Determining Diffusion constants.....	35
5.1.1 Determining the Diffusion coefficients using Matlab.....	35
5.1.2 Diffusion model in Abaqus .....	46
5.2 Determining sample degradation using Abaqus and experiment data for tensile testing	
53	
5.2.1 Material property .....	53
5.2.2 Assembly and step .....	55
5.2.3 Interaction .....	56
5.2.4 Load.....	56
5.2.5 Mesh.....	59
5.2.6 Job and Visualization.....	59
6 Results and Discussion .....	60
6.1 Diffusion model results.....	60
6.2 Tensile test results.....	63
6.2.1 Experimental tensile test results .....	63
6.2.2 Abaqus Tensile Test Result.....	67
7 Conclusion .....	71
8 Bibliography.....	73

Thesis Report	7
Table 1: Typical materials properties for CRPF composite material used for the study .....	20
Table 2: Initial guess of Diffusion parameters, and lower and upper bound limit for the diffusion model in Matlab.....	37
Table 3: Experimental data of diffusion experiment .....	37
Table 4: PDE toolbox basic Function .....	42
Table 5: Optimized Diffusivity values obtained from the Matlab Diffusion Model .....	46
Table 6: Elastic properties used for Diffusion model in Abaqus .....	48
Table 7: Elastic Properties for the Degradation model in Abaqus .....	55
Table 8: Recommendations for future studies .....	70
Figure 1: Optical micrographs are shown for the fractured non-aged_[0] (a), aged_[0] (b), non-aged_[90] (c), aged_[90] (d) tensile coupons [4].....	12
Figure 2:Fickian Diffusion curve for Mass-uptake [6] .....	14
Figure 3: Mechanical properties for aged and non-aged coupes [4] .....	15
Figure 4: Mechanical Properties affected by exposure to different fluid [17].....	17
Figure 5: 2D Sketch of the specimen with dimensions .....	21
Figure 6: Experimental setup for specimen conditioning .....	22
Figure 7: Mass uptake measurement setup.....	23
Figure 8:Tensile testing device .....	24
Figure 9: Data portal for tensile test data .....	26

Thesis Report	<b>8</b>
Figure 10: Data Portal in DIAdem for mass-uptake data .....	26
Figure 11: Fmincon function parameters description [23] .....	29
Figure 12: Flowchart for the determination of Analysis Process .....	34
Figure 13: Flowchart for the Diffusion Model in Matlab .....	35
Figure 14: Mass-uptake curve obtained from experimental data.....	39
Figure 15: Sorption curve (Mass-uptake vs SQRT (time)) [30] .....	40
Figure 16: Isometric view of the Dog-bone 3D part (specimen) used in Abaqus.....	42
Figure 17: Abaqus Modelling process .....	46
Figure 18: Stress-Strain curve of Dry specimens .....	47
Figure 19: Average of Stress-Strain curve for each Orientation type (Dry specimens).....	48
Figure 20: Defining the fiber orientation in Abaqus Modelling .....	49
Figure 21: Defining the Boundary Conditions in Abaqus Model .....	51
Figure 22: Element type selection for mesh elements .....	52
Figure 23: Mesh controls for diffusion model in Abaqus.....	52
Figure 24: Stress-Strain curve for the wet specimens .....	53
Figure 25: Average of Stress-Strain curve all the samples for each fiber orientations .....	54
Figure 26: Constraint definition of rigid body type for the degradation model .....	56
Figure 27: Definition of boundary condition for the degradation model.....	57
Figure 28: Applying the uni-axial Displacement at the one end of the dog-bone 3D part.....	58

Figure 29: Assigning the pre-defined field for the degradation model .....	58
Figure 30: Mesh controls for the degradation model.....	59
Figure 31: Mass-uptake for 0 Degree obtained from experiment, Matlab & Abaqus .....	60
Figure 32: Mass-uptake for 90 Degree obtained from experiment, Matlab & Abaqus .....	61
Figure 33: Mass-uptake for 45 Degree obtained from experiment, Matlab & Abaqus .....	61
Figure 34: Diffusion results in Abaqus .....	62
Figure 35: Experimental Stress-Strain curve for 0° specimen .....	63
Figure 36: Experimental Stress-Strain curve for 45° specimen .....	64
Figure 37: Experimental Stress-Strain curve for 90° specimen .....	65
Figure 38: Experimental Young's modulus comparison between dry and wet specimens .....	66
Figure 39: Max Elongation comparison between dry and wet specimens .....	66
Figure 40: Ultimate Tensile Strength (UTS) comparison between dry and wet specimens .....	67
Figure 41: Load to Displacement comparison for 45° fiber-oriented specimens .....	68
Figure 42: Load to Displacement comparison for 0° fiber-oriented specimens .....	68
Figure 43: Load to Displacement comparison for 90° fiber-oriented specimens .....	69

# 1 INTRODUCTION

---

## 1.1 Background

The composite materials have revolutionized the contemporary engineering products due its superior strength-to-weight ratio, stiffness-to-weight ratio, fatigue properties and toughness. In addition, composites have excellent wear resistance, corrosion resistance and thermal properties. Fiber-reinforced polymer (FRP) composites have long been utilized by several prominent industries including aerospace, marine, civil, automotive, and energy, since they are an attractive alternative for application where metallic materials where traditionally employed [1] [2]. Specifically, the use of composite material in the automotive industry has become even more significant in last few decades.

The modern-day automobiles are required to be increasingly fuel efficient without having any detrimental effect on the performance, and this can be achieved by using the high-performance carbon or glass fiber reinforced polymer (CFRP or GFRP respectively). Although, there is increasing demand of automotive parts made of FRPs, which is likely to rise even higher in future, there are certain limiting factor to its rapid growth in demand. According to Dan Adams, who is a professor at University of Utah and who has achieved great recognition for his research on composites, two of the key limiting factors for abundant use of FRPs in automotive are cost of material and manufacturing [3]. The FRPs are most used in automotive to make structural parts, interiors, powertrain parts, and lubrication system. Particularly, there are a range of powertrain applications where FRP components can be made for instance high-performing seal rings, bearing, shift fork, oil pump, gears, and gear casing to name a few.

Automobile parts such as gearbox and fuel pump, which are made of FRP composite material, will inherently be exposed to working fluid such as lubricating oil, automatic transmission fluid or fuel. This exposure to working fluids might have some long-term unfavorable effects on the material's mechanical, chemical, and thermal properties. These changes in material's properties are due to moisture permeation within the composite material parts that limits their ability to

perform up to its maximum design capacity. There has been considerable amount of research done on the influence of moisture and fluid diffusion on the degradation of composite material. These research works will be thoroughly discussed in the next section, and how it can assist in understand the influence of working fluids on composite gearbox parts.

## **1.2 Objective**

It is evident that the FRP composite parts offer numerous advantages over the conventional metal parts, and to employ FRP material for the use in automotive application for instance its use in gearbox application, it is crucial to understand the behavior of FRP material in an environment and payload like the one that of an operational gearbox. Gearbox parts might be exposed to various operation conditions which includes high cyclic contact stresses, operation in high temperature, and exposure to transmission fluid/gear oil at elevated temperatures. These factors make it even more critical to have proper understanding of FRP composites failure modes in such conditions which would allow the engineers to predict the operational life of parts made out of a composite material. Therefore, the following research questions were raised:

### **1.2.1 Research question:**

1. What are the influences of oil on composite parts used in an automotive industry?
2. How will the influence be determined?
3. If Finite element methods (FEM) modelling is to be used, what model can be used to address the fluid absorption in FRP composite
4. What are the parameters needed for the modelling, and how will they be obtained?
5. Can performing experiments, and using experimental data for the FEM simulation be adequate to study the diffusion behavior in composites?

## 2 LITERATURE REVIEW

---

### 2.1 Influence of working fluid on composite materials

The components used in gearbox typically experience conditions such as high operating temperature, cyclic fatigue load, and exposure to lubricating oil with additives. Moreover, the composite parts used in the gearbox will most likely experience similar environment to composite components used in the oil sector. Some of the key advantages that FRPs offer over metallic material are its resistance to corrosion, excellent wear resistance properties and high strength-to-weight ratio, which allow its application in both automotive and oil industries.

Exposure of FRPs to hygrothermal conditions includes operating in aggressive environment which will cause the composites to undergo some sort of degradation leading to loss of damage tolerance and possibility of pre-mature failure [4]. Furthermore, it is also crucial to understand that the quality of fiber used and the proportion of matrix which will influence the moisture permeation. As mentioned in [4], FRPs made with a high-performance fiber would experience matrix-dominant moisture absorption, nevertheless, the FRPs will experience higher moisture absorption if the fiber used in the FRPs are susceptible to moisture absorption or if its matrix content is high (matrix is also referred to as hygroscopic phase).

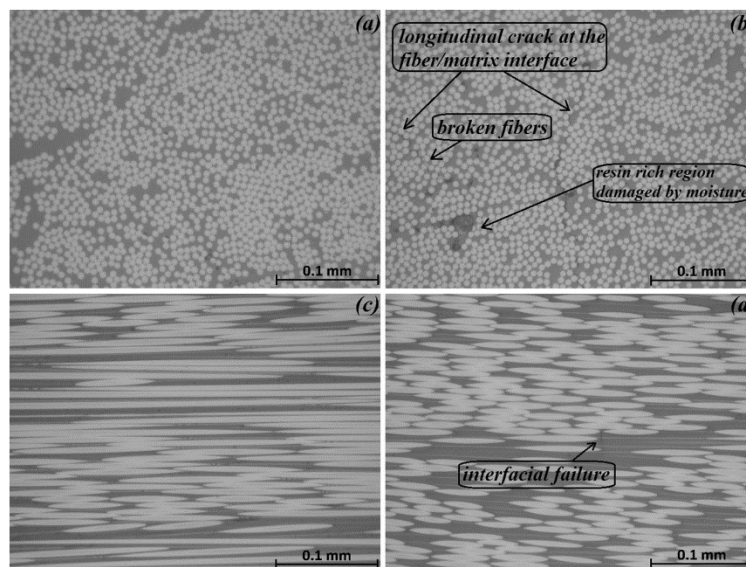


Figure 1: Optical micrographs are shown for the fractured non-aged<sub>[0]</sub> (a), aged<sub>[0]</sub> (b), non-aged<sub>[90]</sub> (c), aged<sub>[90]</sub> (d) tensile coupons [4]

The moisture uptake in FRPs will depend on four key factors which includes micro-cracks, voids, fiber/matrix adhesion, and the matrix and fiber's hydrophilic character [4], and the rate of moisture uptake will vary depending on the type of matrix, fiber, fiber orientation ( $0^\circ$ ,  $45^\circ$ , or  $90^\circ$ ) moisture content, fluid temperature [5]. Figure 1 describes the micrographs of fractured aged and non-aged coupons made of  $0^\circ$  and  $90^\circ$  fiber orientations, and weakening of matrix-fiber interface may have appeared due to the presence of moisture content for the aged coupons [4]. The fluid/moisture enters the composite because of capillary through the cracks and micro-voids which are present close to the fiber and matrix interface, and simultaneously it diffuses through the matrix [6]. However, presence of coupling agent such as silane in a composite material can mitigate the diffusion by constraining the incidence of capillary in the fiber-matrix interface as it provides higher transferability of shear stress between the fibers and matrix. The high transferability of shear stress is crucial to prevent plasticization of matrix which is caused by water absorption. Plasticization might cause permanent damage at the interface and can weaken the fiber-matrix interface and induces the tensile swelling stresses at the phase boundaries [7].

The moisture diffusion is dominant along the fiber direction, and the penetration can be up to 100-400 times faster as compared through the resin. Furthermore, environmental temperature dominates the diffusion rate along the fiber, which means that with increasing temperature in the surrounding, the rate with which diffusion occurs along the fiber direction increases [6] [8] [9]. Also, it should be noted that the hot/wet environment is hostile to the FRPs used parts [8]. Temperature has damaging effect on FRPs, heat combined with moisture can accelerate the deterioration process which can cause permanent structural change at molecular level such as swelling, cracking, plasticization, and debonding of fiber-matrix [10] [11] [4], and additionally, it will result in decrease of the transition temperature of the composites. The moisture diffusion in FRP composites is mainly governed by the Fickian's law of diffusion (refer Figure 2), nevertheless, it may vary from the classical formulation and Non-Fickian diffusion behavior needs to be considered. Therefore, with increasing temperature, the moisture absorption linearly increases with square root of time until it reaches saturation [12] [6].

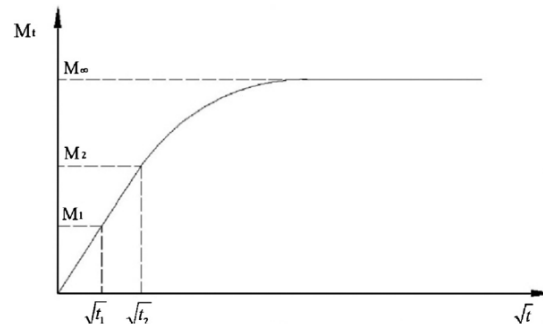


Figure 2: Fickian Diffusion curve for Mass-uptake [6]

Several studies have investigated the influence of various factors which includes exposure to hygrothermal environment, moisture, and humidity on the performance of FRPs. The performance of composites accounted for its fatigue, tensile and compressive behavior, in-plane and interlaminar shear properties, and viscoelastic characteristics. Specific to hygrothermal aging of FRPs, Tsai et al. [13] studied the absorption and diffusion of water in a unidirectional hybrid composite rod specimen made from carbon fiber and glass fiber developed for supporting the overhead conductors. The pre-dried specimens were aged by immersing in water at three different temperatures, 40 °C, 60 °C and 90 °C. It was found that the hybrid FRPs behave in much complex way as compared to single fiber-RP due to the presence of the CF/GF interface which acted as a temporary barrier for moisture absorption between the CF region and GF region. The moisture absorption process followed Fickian diffusion curve for the initial stage of immersion and then diverted as the time progressed. The study concluded that over 77-99 percent of the original thermal and mechanical properties were retained (after drying) as long as the samples retained water concentration in the samples was below the saturation level, minimal damage to the fiber-matrix interface was reported due to the sub-saturation levels of absorbed moisture.

The research article by Jiang et al. [8] presented the gravimetric experiments carried out on GFRP laminates and adhesive of FRP composite bridge which were exposed to hygrothermal aging, and experimental results were compared to FE model of moisture diffusion. The analysis reported that the obtained moisture diffusion coefficient suggested that the moisture absorption due to Fickian diffusion ( $M_{\infty,F}$ ) is humidity-dominant, while the temperature governs the polymeric

relaxation-rate constant ( $k$ ), and elevated temperature significantly accelerates the polymer relaxation process. Finally, it was indicated that 3D moisture diffusion theory is essential to determine the 3D moisture diffusion coefficients of anisotropic FRP composites, and equivalent diffusion coefficient method is unreliable.

Almeida et al. [4] have also performed independent research on the long-term effect of hygrothermal aging and environmental conditioning on tensile, compressive, in-plane shear, and viscoelastic properties of flat filament-wound carbon fiber/epoxy laminates and reported decrease in mechanical properties of the aged laminates. Additionally, the specimen with fiber orientation of  $90^\circ$  fiber orientation was strongly affected by aging due to matrix-dominated failure, while  $0^\circ$  specimens failed due to interlaminar shear with the help of short beam tests, and thus the failure prediction made by Puck's failure criterion was accurate. The difference in mechanical properties of aged and non-aged specimens can be seen in Figure 3.

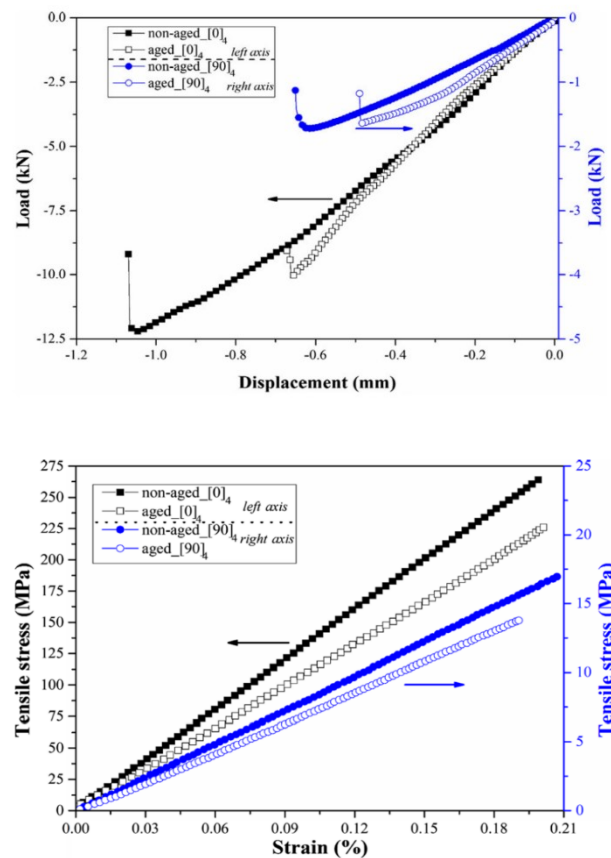


Figure 3: Mechanical properties for aged and non-aged coupons [4]

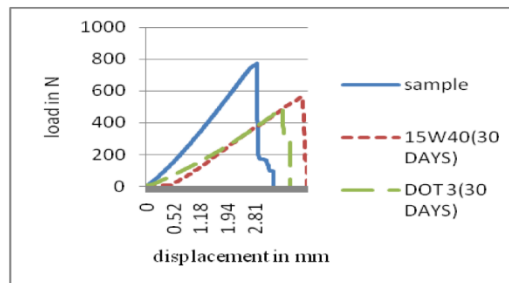
Zafar et al. [14] investigated the long-term effects of moisture on composites made of carbon fiber and epoxy matrix. The specimens were separated immersed in seawater and demineralized water to analyze the moisture uptake behavior and its effect on mechanical properties and glass transition temperature. Furthermore, Raman spectroscopy was also used to study the axial strain of the carbon fiber and transfer of stress through the interface within the composite part. The results showed a general reduction in mechanical and interfacial properties, and the degradation of specimen in immersed in seawater was more severe than demineralized water.

Most of the research performed on the effect of moisture and fluid on composite parts in different testing environments have employed testing fluid as distilled water or sea water. There have been a smaller number of researches where working fluid other than water such as some form of industrial oil have been used to analyze its effect on FRPs. One such study was conducted by Loos A. C. and Springer G. S. [15] where moisture content as a function of time and temperature of three different type of graphite-epoxy composites which were submerged in different fluids including diesel fuel, jet fuel, aviation oil, saturated salt water and distilled water were analyzed (in the range of 300 K to 322 K). Additionally, the effect of humid air with temperature ranging from 322 K to 366 K was also analyzed. The experimental results concluded that samples immersed in diesel fuel, jet fuel, and aviation oil had achieved maximum moisture content around 0.5 to 0.6 percent after 200 days, and the amount of moisture absorption was only time dependent and independent of temperature. However, the moisture absorbed by samples submerged in water showed dependency both on the immersion time and temperature. Lastly, samples exposed to humid air showed dependency only on humidity and was insensitive to temperature, but with very high temperature and moisture level, cracks might form and significantly alter the values of diffusion parameters.

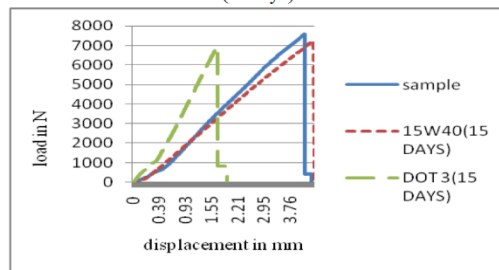
Cherukupally et al. [16] performed research work on the oil diffusion properties of composite foams for oil contaminated water. The experimental data obtained was well described by Sequential dual Fickian (SDF) model which assumes two staged diffusion mechanism. The first stage followed the prediction of Fickian surface diffusion where the improved mass uptake at an equivalent temperature was responsible due to surface wetting and bonding between oil

molecules and polymer. The second stage had much low diffusivities and fraction uptakes which was governed by Fickian physical diffusion or clustering, where the voids, newly formed sites due to swelling, and creeping of a low-viscosity crude filled with cluster of emulsion molecules.

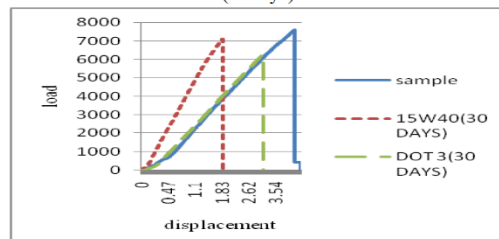
Jayakrishnan et al. [17] studied the effect on flexural and tensile strength of glass fiber/epoxy composite after immersion in universal multi-grade brake oil (20W-40) and in extra high performance hydraulic brake fluid (DOT 3), and most evident effect noticed was weight gain. Additionally, results of oil absorption showed varied effects on other mechanical properties (refer Figure 4, and both solutions had in general degraded the flexural and tensile strength of the specimens, however, it was found that automotive engine had more significant effect on these properties as compared automotive brake oil.



The Effects of Solutions for Bending Specimen (30days)



The Effects of Solutions for Tensile Specimen (15days)



The Effects of Solutions for Tensile Specimen (30days)

Figure 4: Mechanical Properties affected by exposure to different fluid [17]

## 2.2 Modelling

To describe the fluid diffusion process in FRP specimens, different models are considered depending on the requirements and assumptions of the study. Different models have certain assumptions depending on the type of samples being used for the experiment, for instance, description of diffusion process in a homogenized body, non-homogenized body, rigid body, elastic body, or viscoelastic body. Therefore, the past research work that utilized such models to predict the diffusion process in composites must be discussed.

Fan et al. [18] performed research on diffusion of water different in GFRP composite at various temperatures. This paper outline 3 different diffusion models namely Fickian and Spinger diffusion model, coupled deformation-diffusion model and Micromechanics model, and all of these models were used to analyze the experimental data. It was found that the Fickian model can better capture the diffusion behavior in a solid body when the volumetric changes are negligible, while the coupled deformation-diffusion model is ideal to use to capture the volumetric changes in a solid body due to diffusion. The springer diffusion model incorporates fiber volume content but fails to account for the fiber diffusivity. On the contrary, the micromechanical model can account for the effect of fiber volume content and fiber diffusivity along with resin diffusivity, and therefore it allows to model the anisotropic nature of the FRP composites. Thus, due to the versatile nature of the micromechanical model, Gagani et al. [19] have done extensive research work on micromechanical modeling of anisotropic water diffusion in GFRP composite using the 3D anisotropic diffusion theory.

He G. and Liu Y. [20] developed a theoretical model which investigated the mechanical degradation of polymer composites due to moisture absorption by employing internal state variable (ISV) theory. Furthermore, Huo et al. [2] investigated the mechanical degradation of carbon/bismaleimide composites exposed to seawater conditioning with the help of 3D moisture diffusion modelling.

## **3 SPECIMEN USED AND EXPERIMENTAL METHODOLOGY**

---

The primary goal of the research project is to determine how the composites behave when exposed to a working fluid such as oil. The goal is to measure the effect such as diffusion of fluid particle in composite part and model it. To address this, the following two experiments were set-up:

1. Measure the mass uptake of oil into the material.
2. Compare the dry and oil exposed material's properties with performing tensile tests.

From the obtained mass-uptake data, diffusion parameters such as diffusivities and solubility are to be estimated using Matlab. The obtained parameters from the Matlab were then used to simulate diffusion in Abaqus. The diffusion analysis in Abaqus is used to validate the Matlab's FEM model, and the obtained output field of normalized concentration is used as an input to static general simulation. Due to diffusion of oil in composite part, the mechanical properties of the oil exposed specimens are dependent on mass concentration which were measured by tensile tests. Lastly, the experimentally obtained mechanical properties were compared to simulated mechanical properties obtained by FEM model in Abaqus.

### **3.1 Specimen Material**

The specimens which will be used for the experiments were manufactured using 3D printer, therefore it was crucial to choose a material for the specimens which had to be specifically functional to 3D printing task. Thus, the ColorFabb XT-CF20 was chosen to be the suitable material for the 3D printing tasks. The selected material is an engineering grade 3D printing filament based on Eastman chemical amphora (AM1800) 3D polymer which is strong and definitive in its characteristic. According to the colorfabb instructions, it was suggested that the 3D printing temperature must be with 240-260 °C, the 3D printing speed advised to be within 40-70 mm/s, and the temperature range for the heated bed must be within 60-70 °C. In addition,

the continuous service temperature was prescribed to be 75 °C which was one of the constraints of the experimental setup. Considering the limitation of the continuous service temperature, the service temperature of the oil diffusion experiment was taken as 60 °C for the purpose of conditioning the specimens [21].

Some of the key features of the ColorFabb XT material contains short carbon fiber which has high strength and extremely good toughness, odor neutral processing, high Tg or improved temperature resistant properties, and Styrene and BPA free formulation. Below are the key materials physical properties obtained from the technical data sheet of ColorFabb [21].

*Table 1: Typical materials properties for CRPF composite material used for the study*

<b>TYPICAL MATERIAL PROPERTIES [21]</b>			
<b>Physical Properties</b>	<b>Unit</b>	<b>Value</b>	<b>Method</b>
<b>Humidity absorption (23°C,50%RH)</b>	%	---	
<b>Tensile Strength</b>	MPa	76	ISO 527
<b>Tensile Elongation@break</b>	%	7,5	ISO 527
<b>Flexural Strength</b>	MPa	110	ISO 178
<b>Flexural Modulus</b>	GPa	6,2	ISO 178
<b>Izod Impact strength, notched</b>	kJ/m <sup>2</sup>	6	ISO 180
<b>Izod Impact strength, unnotched</b>	kJ/m <sup>2</sup>	60	ISO 180

### 3.2 Specimen Shape and Dimension

The 3D printed specimens were designed to be in an “I” shaped which were 3.2 mm thick. This shape was adopted because it would enable easy handling of the specimens when tensile testing would be performed on the it. The detailed sketch of the shape and the dimensions which were used to 3D print the specimens is shown below in Figure 5:

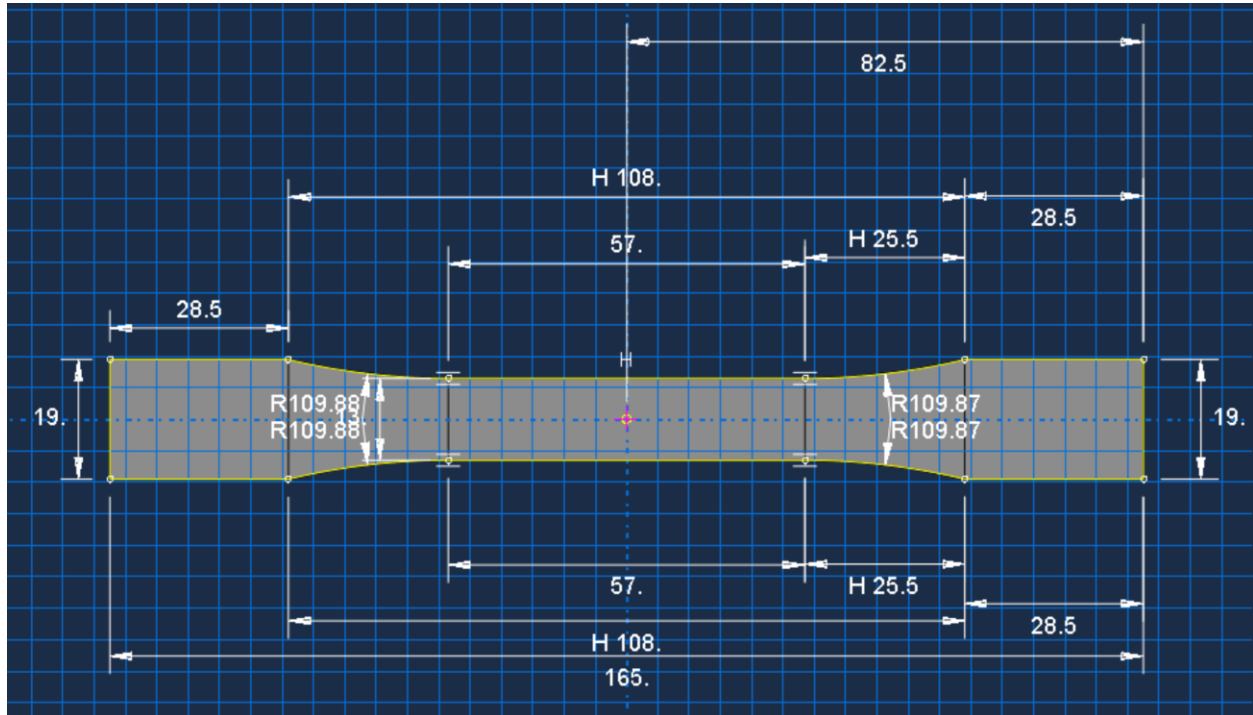


Figure 5: 2D Sketch of the specimen with dimensions

There were 3 types of samples created using 3D printer which included fiber direction in 0, 45, 90. Additionally, in total 60 samples were 3D printed for the purpose of oil and thermal conditioning where a set of 10 samples had identical fiber orientations for each of the above-mentioned sample types respectively. Making a total of 10 specimens of each orientation type was decided to account for any variations in experimental data.

### 3.3 Experimental Methodology

#### 3.3.1 Conditioning the 3D printed composite samples

In order to analyze the samples, 30 samples (3 sets of 10 samples for each fiber orientation type) were separated for conditioning, and the other 30 samples were for the purpose of tensile testing of the unconditioned specimens for respective fiber orientation type. To condition the samples, a closed system experimental setup was created under oil which was always regulated to be at 60 °C with the help of heating plate. The experimental setup for conditioning is shown below in the Figure 6 and Figure 7, where different components of the setup are listed. The oil in which the specimens were conditioned was Paramo CLP 100 ISO VG 100 which is chiefly used as a lubricating oil for industrial gearboxes where high stresses and gear pressures are involved, and it can also be used for bearings and other moving parts where high-pressure oil properties are critical [22].

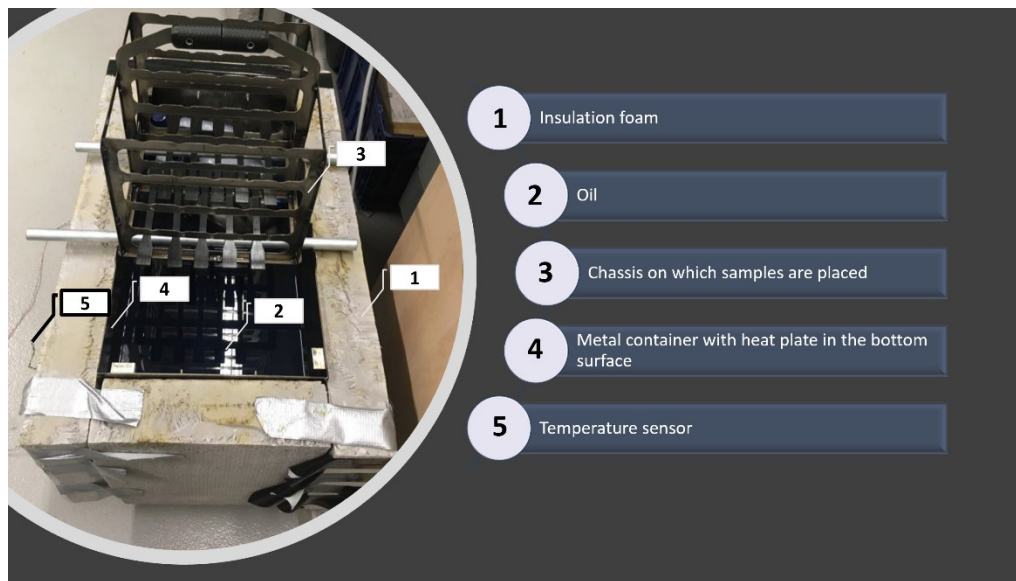


Figure 6: Experimental setup for specimen conditioning

As part of the experiment to determine the diffusion properties such as diffusivity and solubility of the 3D printed samples, the specimens were fully submerged in the hot oil for a period of 2966 hours. In addition, to monitor the mass uptake during the diffusion process, the samples were taken out on a regular basis, dried, and then weighed on a high precision weighing scale, and the mass of the samples were noted respectively.



Figure 7: Mass uptake measurement setup

### 3.3.2 Tensile testing

The tensile test was performed two times, where the first test was performed prior to the samples being conditioned, and the second test was performed on the wet samples. The test was performed on the Biaxial Testing Machine for Biaxial Tensile Tests which is designed for obtaining material characteristics of both standard materials and composite materials for use in engine design at the CVUT university laboratory (Figure 8).



*Figure 8:Tensile testing device*

For the dry samples testing, the 30 unconditioned samples were used to perform the tensile test to obtain the data which would be used to determine the materials properties of the specimens which will be useful in the analysis section for the comparison of conditioned and unconditioned specimens. Similarly, the 30 samples which were exposed to oil were used to perform tensile testing, and the obtained data was used to analyze the degradation effect of oil on the samples.

## 4 PROGRAMS AND MATHEMATICAL EQUATIONS

---

### 4.1 Diadem-NI and Excel

Due to the larger number of samples, the data obtained for the mass uptake and tensile testing was enormous and performing all the data processing in Excel would require comparatively more time. Therefore, NI-DIAdem was employed as it offered enhanced post-processing capabilities with the help of script writing.

The raw data obtained from the laboratory needed to be sorted a first before it could be used in the DIAdem which was performed with the help of MS Excel. Once the data was sorted, it was imported in DIAdem where the Navigator panel allowed for easy import of sorted data file. The DIAdem's data portal imports the data which consist of groups that contains number of channels depending on how the data needs to be configured. With the help of DIAdem scripting, the mass-uptake data was processed to obtain the relative mass-uptake values of the 3D printed composite specimens, where the following formula was used to obtain the relative values for all the samples respectively:

$$\text{Relative Mass uptake} = \frac{(M_i - M_0)}{M_0} \quad (1)$$

Where,  $M_i$  is Current Weight of the sample at time t; ,  $M_0$  is the weight of the sample at time t=0.

After the relative values were obtained corresponding to the time for each sets of measurements, these values were sorted using the Diadem scripting as shown in the Figure 10 below. Ultimately, the 10 values of each specimens were averaged for all measurements as shown in the second part of the Figure 10.

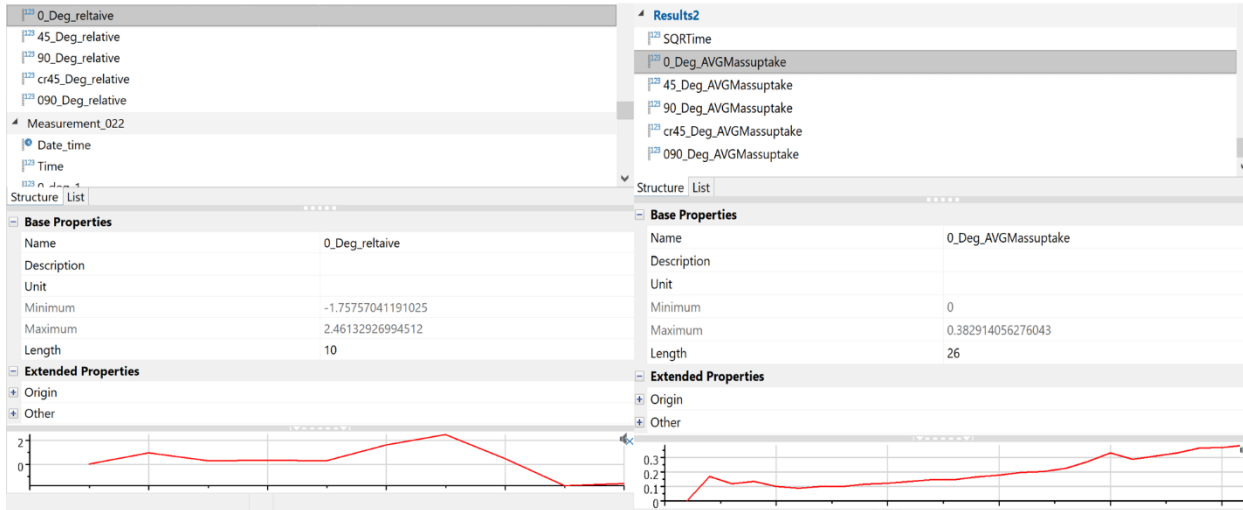


Figure 9: Data Portal in DIAdem for mass-uptake data

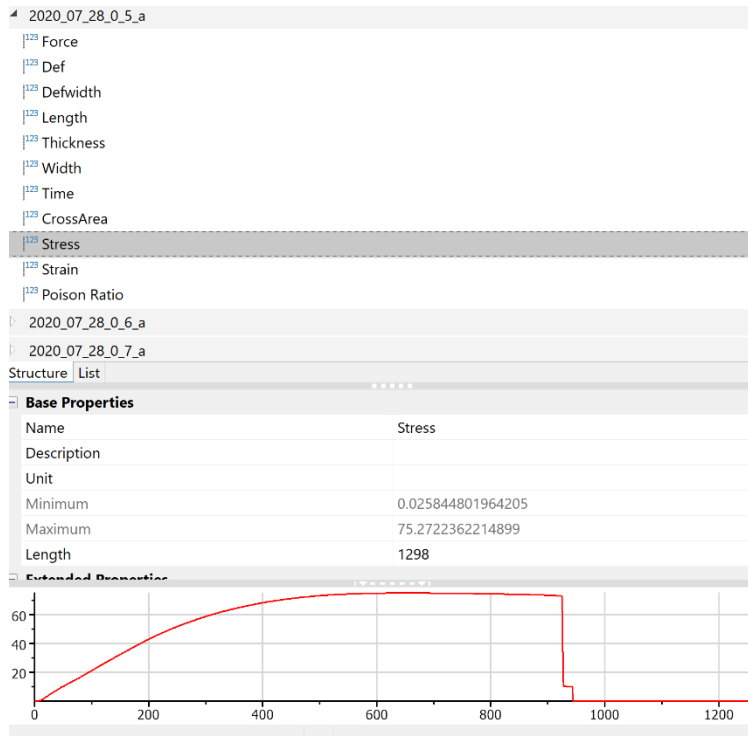


Figure 10: Data portal for tensile test data

Once the average mass-uptake values for the all the specimens were obtained for all specimen types including 0°, 45°, 90° fiber orientation, using the “REPORT” panel of the DIAdem, the plots for the Mass uptake versus time were plotted for different fiber orientation.

Similar approach was used to perform data processing for the tensile testing of the unconditioned and conditioned specimens, and the data was processed have the setup for data channels for each reading for the respective specimen type as shown in the Figure 9.

The raw data obtained from the tensile test experiment were processed via DIAdem scripting to obtain the value of stress, strain, Poisson’s ratio, the Young’s Modulus, and Shear Modulus. The equations used to calculate are given below:

$$\text{Stress, } \sigma = \frac{\text{Force}}{\text{Area}} = \frac{\text{Force}}{(\text{Width}_{\text{specimen}} * \text{Thickness}_{\text{specimen}})} \quad (2)$$

$$\sigma = \left[ \frac{N}{\text{mm}^2} \text{ or } \text{MPa} \right]$$

$$\text{Strain, } \varepsilon = \frac{\Delta L (\text{change in length})}{L (\text{Length})} \quad (3)$$

$$\text{Young's Modulus} = \frac{\text{Stress}}{\text{Strain}} = \frac{\sigma}{\varepsilon} [\text{MPa}] \quad (4)$$

$$\text{Shear Modulus} \sim 60\% * \sigma [\text{MPa}] \quad (5)$$

$$\text{Poisson's Ratio} = \frac{\varepsilon_{\text{Lateral Strain}}}{\varepsilon_{\text{Longitudinal Strain}}} \quad (6)$$

With the help of DIAdem, the values of stress, strain, and Poisson’s ratio were calculated, and MS Excel was used to determine Young’s Modulus and Shear Modulus using the plot of stress versus strain for all the specimens for each type of fiber orientation.

## 4.2 Matlab

The Matlab was used to estimate the diffusion parameter values such as the diffusion constants ( $D_{11}$ ,  $D_{22}$  and  $D_{33}$ ) and solubility using the 3D mass uptake section 4.1. Matlab scripting was used to write a code which would call several user defined functions to ultimately calculate the mass uptake value for a given time. The experimental data of mass uptake was used for the following reasons:

- To obtain an array of time which would be used in the mass uptake equation where the time array was obtained by calculating the number of hours between each measurement were taken in the laboratory. The time calculations were performed in MS Excel where time intervals were determined. In total 26 measurements were taken which means the Matlab script had a time array consisting of 26-time intervals.
- The values of experiment mass uptake were used to compare with the simulated values of mass uptake values using the 3D Mass uptake equation, and to estimate the squared error value to perform the optimization routine.

The values of diffusion parameters were estimated using two different approaches including the use of optimization toolbox and the use of curve fitting toolbox.

The optimization toolbox offers multiply ways to optimize a parameter by maximizing or minimizing objective while satisfying constraints. Some the solvers that are included in the toolbox are linear programming (LP), mixed-integer programming (MILP), Quadratic programming (QP), nonlinear programming (NLP), constrained liner least squares, nonlinear least squares, and nonlinear equations. One of the features of the toolbox is that design optimization tasks can be performed which includes parameter estimation, component selection, and parameter tuning. In particular, to estimation of diffusion parameters in Matlab, “fmincon” function of the optimization toolbox was employed.

As the name suggest, fmincon function determines the minimum of a constrained nonlinear function, and the syntax of the function is given below [23]:

$$x = \text{fmincon}(\text{fun}, x_0, A, b, A_{\text{eq}}, b_{\text{eq}}, lb, ub, \text{nonlcon}) \quad (7)$$

Where, it subjects the minimization to the nonlinear inequalities  $c(x)$  or equalities  $ceq(x)$  defined in *nonlcon*.

*fmincon* optimizes such that  $c(x) \leq 0$  and  $ceq(x) = 0$ . If no bounds exist, set  $lb = []$  and/or  $ub = []$ .

$$x = \text{fmincon}(\text{fun}, x_0, A, b, A_{\text{eq}}, b_{\text{eq}}, lb, ub, \text{nonlcon}, \text{options}) \quad (8)$$

Where, it minimizes with the optimization options specified in *options*. Use *optimoptions* to set these options. If there are no nonlinear inequality or equality constraints, set  $\text{nonlcon} = []$ .

There are many more syntax of this function and depending on the application the above two syntax were appropriate for the estimation of mass diffusion parameters. The given Figure 11 below describes the problem structure of *fmincon* function:

Problem structure, specified as a structure with the following fields:

Field Name	Entry
objective	Objective function
x0	Initial point for x
Aineq	Matrix for linear inequality constraints
bineq	Vector for linear inequality constraints
Aeq	Matrix for linear equality constraints
beq	Vector for linear equality constraints
lb	Vector of lower bounds
ub	Vector of upper bounds
nonlcon	Nonlinear constraint function
solver	'fmincon'
options	Options created with <a href="#">optimoptions</a>

You must supply at least the objective, x0, solver, and options fields in the problem structure.

Data Types: struct

Figure 11: *Fmincon* function parameters description [23]

#### 4.2.1 Mathematical equations used for the Diffusion analysis

During the process of specimen conditioning under oil and at some elevated constant temperature, the diffusion of mass into the specimens have been assumed to be following the Fick's law. The detailed information has been described in the subsections below.

#### 4.2.1.1 Fick's 1st Law.

Fick's 1<sup>st</sup> law describes that in a diffusion process of molecules, the diffusive flux is proportional to the concentration gradient as it travels from high concentration to low concentration. In other words, the flux is the rate of change of concentration with respect to position [24].

$$J = -D \frac{\partial C}{\partial z} \left[ \frac{1}{mm^2hr} \right] \quad (9)$$

Where, J is Diffusion Flux.

$$D = \text{Diffusivity} \left[ \frac{mm^2}{hr} \right] \quad (10)$$

Where, J is Diffusive Flux and C is Concentration in mass unit per unit length.

#### 4.2.1.2 Fick's 2nd Law.

The 2<sup>nd</sup> law is derived from the 1<sup>st</sup> law; however, it accounts for the change in concentration with time. The local concentration and diffusion through an area A and position z can be written as C(z, t), J(z), through which the following equation can be written:

$$\frac{\partial C(z, t)}{\partial t} = - \frac{\partial J}{\partial z} \quad (11)$$

Subbing the 1<sup>st</sup> law in the above equation.

$$\frac{\partial C(z, t)}{\partial t} = D \frac{\partial^2 C}{\partial z^2} \quad (12)$$

Where C is concentration, D is diffusivity, and z is distance in space.

For the 3D space, the equation can be written as given below:

$$\frac{\partial C}{\partial t} = D \nabla^2 C \quad (13)$$

#### 4.2.2 Calculations of diffusion parameters $D_{11}$ , $D_{22}$ , $D_{33}$

The above 3D mass diffusion equation has been used for the analysis. Where  $D_{11}$ ,  $D_{22}$ ,  $D_{33}$  are the orthotropic diffusion constants and accounts for diffusivity in x, y, and z direction or across length, width and height of a sample object where the diagonal terms have been ignored. Section 4.2.2 discussed how these parameters will be estimated using Matlab in detail.

$D_{\parallel} = D_{11}$  is the diffusivity in the direction of printing of the fiber.

$$D_{\perp} = D_{22} = D_{33} \quad (14)$$

$D_{\perp}$  is the Diffusivity perpendicular (across width or thickness) to the direction of the fiber.

There were 3 key computer software used for the purpose of post-processing the experimental data and its analysis, and for the simulations. To be specific, the post-processing of experimental data of mass uptake and tensile testing were performed primarily in diadem and MS Excel due to its excellent data processing capabilities. With post processed data obtained, the theoretical diffusion model was formed in Matlab which was used to determine the optimized diffusion parameters. Finally, Abaqus was used to perform FEA modeling whose results were used for the comparison between experimental and simulated data.

#### 4.2.3 Moisture uptake and Moisture Saturation Content

During the diffusion process, the mass uptake through a surface or into an object will reach a saturation point when the concentration gradient reaches to its minimum value ( $\approx 0$ ). It can be explained by looking at the gravimetric curve in the Figure 2 which also illustrates the theoretical Fickian diffusion process.

The gravimeter curve can be obtained by using the following moisture uptake equation, which was used to obtain the Mass uptake value from the experimental data which has been discussed in section 4.2.1:

$$M_t = 100 * \left( \frac{w_t - w_0}{w_0} \right) \quad (15)$$

The saturation level can be the maximum value of moisture uptake, or the mass uptake value when the difference in the two consecutive measurements is lower than 0.5%.

### 4.3 Abaqus

Performing the FEA analysis using the 3D Diffusion equation and other analytical approach to obtain diffusion parameters manually is possible, but it is a griming task and is time demanding. Using computer software like Abaqus CAE to perform Finite element analysis (FEA) analysis a common approach that engineers use these days as achieving precise results is possible and the computing time is relatively minimal in comparison to performing hand calculations. By implementing FEA solutions with the help of finite element equations, the moisture concentration value can be estimated within a component using a discrete model made up of continuous functions identified using finite number of elements in parts [25].

#### 4.3.1 Governing equation in Abaqus CAE for Diffusion model

In Abaqus CAE, Mass diffusion analysis can perform modelling for both steady-state and transient diffusion process, and it requires the use of mass diffusion elements. In addition, it is possible to model temperature, concentration, and/or pressure gradient-driven mass diffusion. mass diffusion equation is an extension of Fick's law of diffusion which allows for the nonuniform solubility of the diffusing substance. The "normalized concentration" is the basic solution variable which is used at the nodes of the mesh as the degree of freedom, and the normalized concentration is continuous across the interface between the dissimilar materials, when a mesh includes different materials with shared nodes. The equation below illustrates that as [26]:

$$\phi \stackrel{\text{def}}{=} \frac{C}{S} \quad (16)$$

Where C is the mass concentration of the diffusing material [parts per million or P]

$$S = \text{Solubility} [PLF^{\frac{1}{2}}, F \text{ is force}, L \text{ is length}] \quad (17)$$

In Abaqus, the diffusion problem requires to follow the mass conservation for the diffusing phase, and the respective equation is given below:

$$\int_V \frac{dC}{dt} dV + \int_S n \cdot J dS = 0 \quad (18)$$

Where V is volume, S is surface, J is flux of concentration of the diffusing phase, and n\*J is concentration flux leaving S.

Using Fick's first law and the assumption that the diffusion is driven by the gradient of general chemical potential, the following equation is derived:

$$J = -SD \cdot \left[ \frac{\partial \phi}{\partial x} + \kappa_s \frac{\partial (\ln(\theta - \theta^Z))}{\partial x} + \kappa_p \frac{\partial p}{\partial x} \right] \quad (19)$$

where D is diffusion constant, S is solubility,  $\theta$  is temperature,  $\theta^Z$  is the absolute zero on temperature scale being used, and  $\kappa_s$  is "Soret effect" factor which provides diffusion due to temperature,  $\kappa_p$  is the pressure stress factor provided the diffusion is driven by gradient of equivalent pressure. P represents the  $-\text{trace}(\sigma)/3$ . Lastly, it should be noted that the problem becomes nonlinear, and the system of equations becomes nonsymmetric when the D,  $\kappa_p$ , or  $\kappa_s$  depends on concentration which is the usual case in real world. Therefore, while performing diffusion analysis, the nonsymmetric matrix storage and solution scheme is invoked automatically [26]. The pressure driven diffusion and temperature driven diffusion is not considered to be accountable as part of the study which will result in  $\kappa_p = \kappa_s = 0$ , therefore, the Abaqus's governing equation narrows down to the Fick's second law equation.

## 5 ANALYSIS

To demonstrate the analysis method, the Figure 12 contains a flowchart which summarizes the flow structure of the analysis.

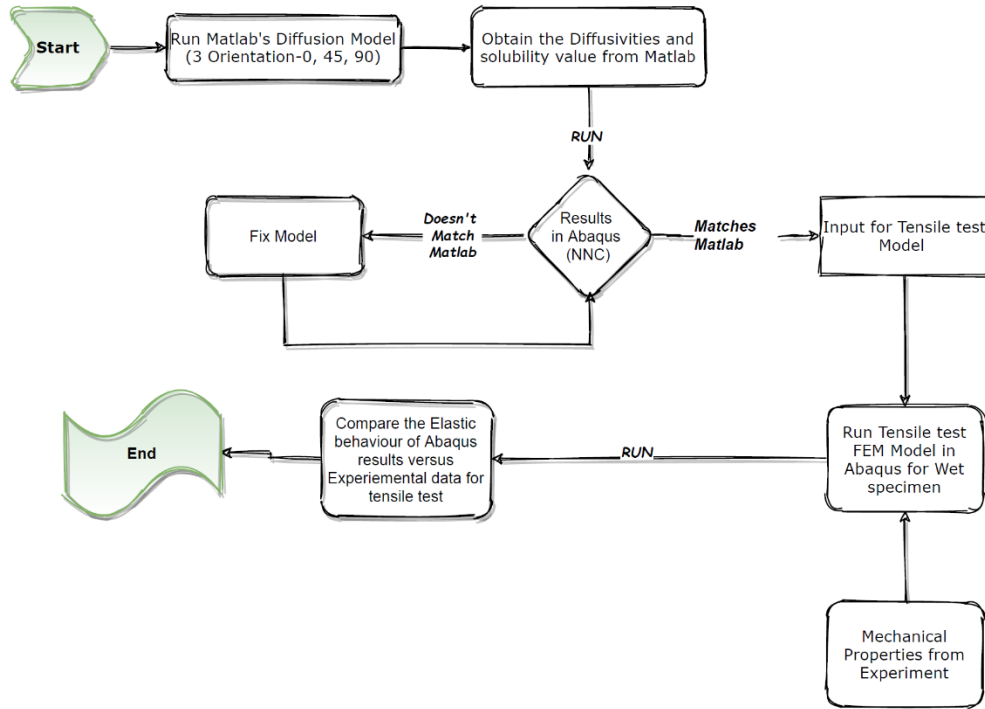


Figure 12: Flowchart for the determination of Analysis Process

## 5.1 Determining Diffusion constants

### 5.1.1 Determining the Diffusion coefficients using Matlab

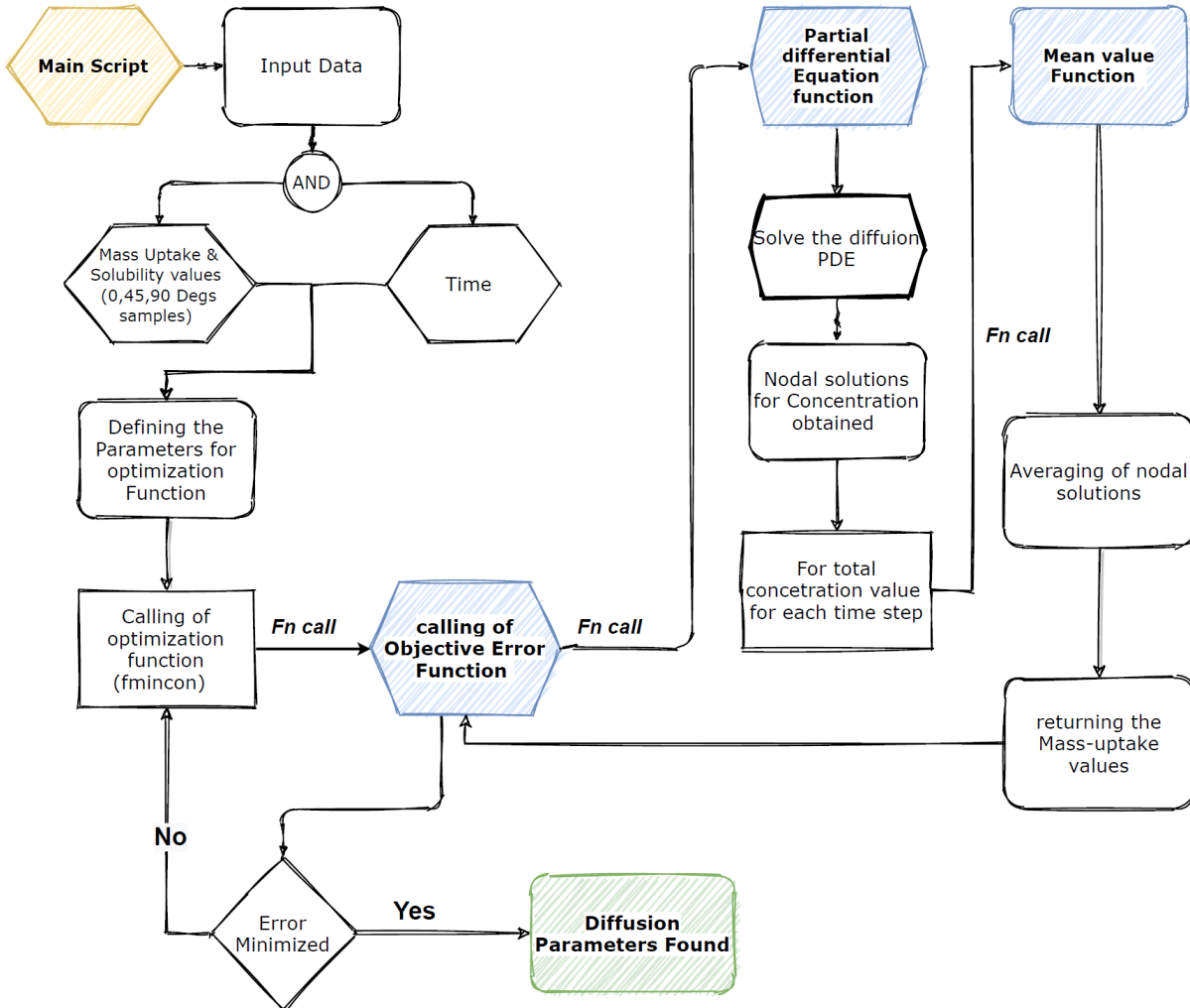


Figure 13: Flowchart for the Diffusion Model in Matlab

The Figure 13 presents a flowchart which graphically characterizes the stepwise process when the Matlab script is run to simulate the diffusion model which was made with the help of Finite

element method. The primary aim of the Matlab model was to simulate the mathematical model and find the optimized values of diffusivities (D11, D22 and D33) and Solubility for the specimens.

The Matlab model consists of a main script (.m file) which employs three user defined functions as the script demands. The three functions are listed below:

- ◆ Objective error function
- ◆ PDE function
- ◆ Mean value function

#### ***5.1.1.1 Application of fmincon function for optimization***

As its mentioned above, the Matlab model aims to deliver the optimized values for the diffusivities and solubility, section 4.2 of this report briefly describes the use of fmincon function of the optimization toolbox to achieve this objective. The task of fmincon function for this study was to minimize the value returned by the objective error function. As described in section 4.2, fmincon functions requires several inputs of which includes the most crucial input values are listed below:

- ◆ “@Objective”: Objective error function
- ◆ “x0”: p1 array which includes the initial assumed values of diffusivities (D11, D22, D33) and solubility (Msat-saturation value)
- ◆ “lb”: lower bound limit for the p1 array
- ◆ “ub”: upper bound limit for the p1 array

From the above lists, the “lb” and “ub” array is extremely crucial as the respective optimized values obtained will be within the assumed lower and upper bound limit, and if assumed wrong can yield false or inaccurate results. Additionally, while performing the analysis, the effect of lower and upper bound values for optimized result was also performed and the optimum values are described in the Table 2 with the values for the other input variables

Table 2: Initial guess of Diffusion parameters, and lower and upper bound limit for the diffusion model in Matlab

<b>Fmincon input variable</b>	<b>D11</b>	<b>D22</b>	<b>D33</b>	<b>Msat</b>
<b>"x0"</b>	0.00803	0.0075	7.5E-05	0.691
<b>"lb"</b>	0.001	0.004	0.0001	0.3
<b>"ub"</b>	0.9	0.9	0.009	1

In addition, to the above-mentioned input variables, another set of data which was experimentally obtained was also part of the input data, nevertheless, it was mainly used to obtain the squared error between the experimental and simulated values. These input data included in the script consisted of relative mass uptake value and time array that contains the list of times at which the mass-uptake readings were collected for each sample types experimentally, as mentioned in section 4.2. The experimentally data obtained was processed in Diadem, and the values are presented in the Table 3.

Table 3: Experimental data of diffusion experiment

<b>0 Degree</b>	<b>45 Degree</b>	<b>90 Degree</b>	<b>Time</b>
-5.93E-09	-5.58E-08	1.30E-07	0
-0.05929	-0.05578	0.13047	15
-0.03821	-0.05754	0.143891	42
-0.05652	-0.0754	0.239819	109.5
-0.07514	-0.06571	0.202445	163.5

-0.06384	-0.08863	0.255142	205.5
-0.0583	-0.08711	0.289787	302
-0.03943	-0.06766	0.372738	398
-0.03156	-0.03311	0.386404	446.2833
-0.02109	-0.01682	0.45667	520
-0.01063	-0.00499	0.455625	615
-0.01508	0.002089	0.454693	686
-0.00014	0.021961	0.50167	783
0.014236	0.037264	0.504191	951
0.034262	0.06558	0.550672	1119
0.042976	0.077194	0.562807	1213.833
0.064907	0.09471	0.603067	1381
0.108841	0.123857	0.62095	1550
0.193181	0.145505	0.638351	1717
0.143186	0.122369	0.617117	1889.5

0.157203	0.142711	0.647017	2034
0.206163	0.156769	0.686058	2227.5
0.238539	0.161585	0.67573	2395
0.257232	0.147621	0.661902	2558
0.277881	0.15647	0.689233	2798
0.337444	0.186005	0.691221	2966

In addition, the graphical representation for the mass-uptake trend over a period for each sample types are presented in Figure 14:

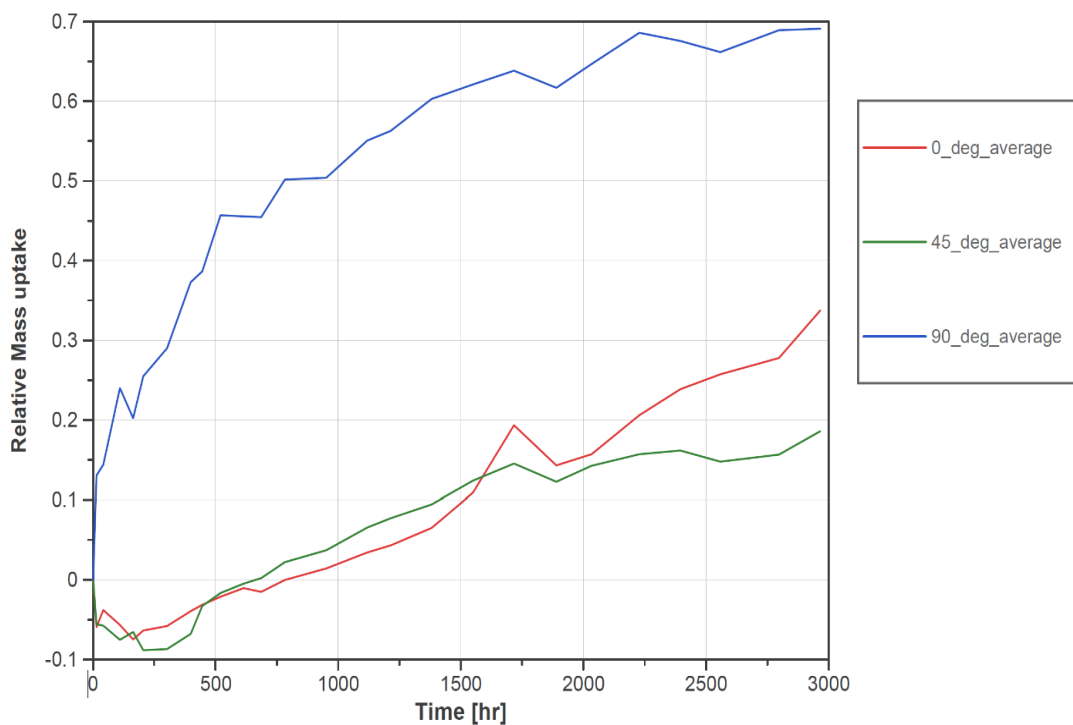


Figure 14: Mass-uptake curve obtained from experimental data

As it can be seen in the above Figure 14, the experimentally obtained data have irregularities with the theoretically predicted data where a mass uptake data should follow an exponential function until it reaches a saturation value, as shown in Figure 15 which shows a typical mode of transport for two different sorption cases:

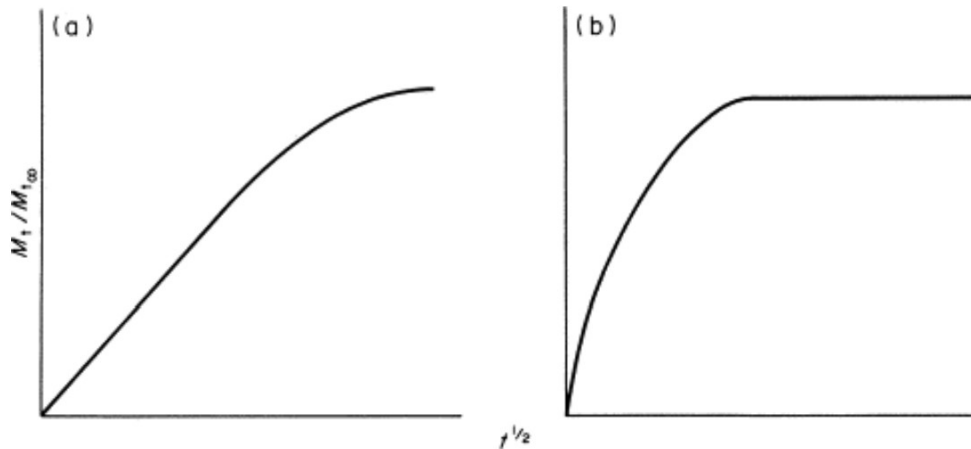


Figure 15: Sorption curve (Mass-uptake vs SQRT (time)) [30]

However, among the obtained data for different specimen type, only samples with 90-degree fiber orientation resemble the expected trend, while the mass-uptake data for samples with 0- and 45-degree fiber orientation showed initial negative values (which represents loss of mass), for the initial period of experimental measurements. This could possibly be due to human error while handling the samples. Additionally, the drying of the samples was manually performed instead of using a hot air oven or similar drying device which could have contributed to the irregularities in the experimental data.

### 5.1.1.2 Analyzing the squared error

To obtain the optimized parameters via `fmincon` function, user defined Matlab function called objective error function which evaluates the error between experimentally measured relative mass uptake values and analytically calculated mass uptake values. The following equation was used to determine the squared error value:

$$e1 = \sqrt{\left(\sum_{i=1}^{26} \left(\frac{Mtsim_i - Mtmeas0_i}{Mtmeas0_i}\right)^2\right)} \quad (20)$$

$$e2 = \sqrt{\left(\sum_{i=1}^{26} \left(\frac{Mtsim_i - Mtmeas45_i}{Mtmeas45_i}\right)^2\right)} \quad (21)$$

$$e3 = \sqrt{\left(\sum_{i=1}^{26} \left(\frac{Mtsim_i - Mtmeas90_i}{Mtmeas90_i}\right)^2\right)} \quad (22)$$

$$error = \sqrt{e1^2 + e2^2 + e3^2} \quad (23)$$

Where Mtmeas0, Mtmeas45, and Mtmeas90 are experimental values of mass uptake for 0°, 45°, and 90° fiber-oriented samples respectively, and Mtsim represents the simulated mass uptake values.

### ***5.1.1.3 Simulating the mass-uptake values using the PDE toolbox***

To obtain simulated mass uptake values, objective error function would call user defined PDE function which uses the Matlab's partial differential equation toolbox. The functionality of this toolbox is to solve problems of structural mechanics, heat transfer, and general partial differential equations with the help of finite element analysis. It enables the user to perform FEA analysis in Matlab which provide comparable results to CAE software like Abaqus and Ansys. The versatility and simplicity of the PDE toolbox enabled the import of 3D geometry of the testing specimen to pde model [27]. The 3D geometry was created in Solidworks using the dimensions mentioned in section 3.1 of this report, and the Figure 16 describes the 3D shape from Solidworks.

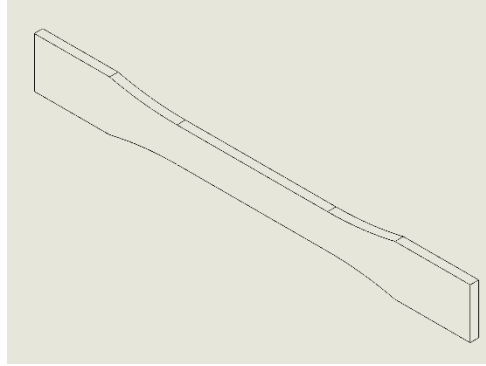


Figure 16: Isometric view of the Dog-bone 3D part (specimen) used in Abaqus

To solve general PDE or a system of PDEs, the workflow consists of following steps [27]:

- ◆ Convert PDEs to the form required by Partial Differential Equation Toolbox.
- ◆ Create a PDE model container specifying the number of equations in your model.
- ◆ Defining 2-D or 3-D geometry and mesh it using triangular and tetrahedral elements with linear or quadratic basis functions.
- ◆ Specify the coefficients, initial conditions, and boundary conditions. Use function handles to specify non-constant values.
- ◆ Solve and plot the results at nodal locations or interpolate them to custom locations.

Additionally, the pde Model setup consists of the following Matlab function (Table 4):

Table 4: PDE toolbox basic Function

<b>PDE toolbox basic functions for creating FEM model</b>	
<b>createpde</b>	Create model
<b>applyBoundaryCondition</b>	Add boundary condition to PDEModel container
<b>specifyCoefficients</b>	Specify coefficients in a PDE model

<b>setInitialConditions</b>	Give initial conditions or initial solution
<b>assembleFEMatrices</b>	Assemble finite element matrices
<b>solvepde</b>	Solve PDE specified in a PDEModel
<b>solvepdeeig</b>	Solve PDE eigenvalue problem specified in a PDEModel

Once the pde model is created and the specimen geometry has been imported using the toolbox's import command, the next step was to initialize the coefficients of the diffusion equation. The toolbox addresses the following general equation: 4.2.1.2

$$m \frac{\partial^2 C}{\partial t^2} + d \frac{du}{dt} - \nabla(c \nabla u) + au = f \quad (24)$$

Where  $m$ ,  $d$ ,  $c$ ,  $a$  are coefficients whose value must be user defined, and  $u$  represents concentration value.

The above equation represents the convection and diffusion transport term, however for the relevance of this study, only diffusion transport is responsible for the transport mechanism of oil into the samples. Considering the conditions for the analysis, the following values were taken for the above-mentioned coefficients:

<b>PDE toolbox coefficients values</b>	
<b>'m'</b>	0
<b>'d'</b>	1

'a'	0
'c'	Input values of D11, D22, D33 from the fmincon function
'ϕ'	0

Applying the above coefficients to the equation will yield the following formula which will be used to simulate the mass-uptake values:

$$\frac{du}{dt} = \nabla(c\nabla u) \quad (25)$$

The above equation is same as the basic diffusion equation mentioned in the section 4.2.1.2 of this report.

The next step was to define the boundary conditions using the `setInitialCondition()`. The PDE toolbox offers possibility of defining boundary conditions, first one being Dirichlet conditions or Neumann conditions. For analysis purposes, it was decided that assigning Dirichlet boundary conditions was more suitable because transport mechanism is primarily driven by concentration-based diffusion process. The boundary conditions were assigned to all the outer faces of the 3D model, and the following formula is used by the toolbox:

$$h * u = r$$

where  $h$  and  $r$  are constants which user must define, and  $u$  is the concentration value.

The values for the above constants were taken as follows:

$$h = 1$$

$$r = 1$$

The reason behind assigning 1 for each constant was that the value of normalized concentration would then be equal to 1 at all the faces of the specimen which would explain the experimental setup condition where the samples were fully submerged in the oil.

Lastly, the mesh was generated using the `generatemesh()`, and the diffusion partial differential equation was solved using the `solvepde()` command. The maximum mesh size was defined to be as two, it could have been lower number which would mean more fine mesh, and the convergence would be enhanced, but it would mean higher computing time. Lastly, in regard to the solving the respective PDE problem, the time array obtained while taking the experimental data, and which is mentioned in the Table 3, was used as an input so the solution (mass-uptake value at each node) would be relative the experimental times at which measurements were conducted. Thus, it would enhance the legitimacy of the obtained results.

The solution obtained by solving the diffusion pde function was in the form of nodal solutions. Each time step from the time array would have same number of solutions as number of nodes on the meshed geometry. To obtain a mass-uptake value for the entire 3D geometry, mean value of all the nodal solutions for each timestep was calculated using a separate user-defined Matlab function called "meanval". Lastly, the time array consisted of 26 values, thus the obtained simulated mass-uptake values same as number of experimentally measured mass-uptake values thus, objective error function can compute the error which is optimized by the `fmincon` function.

### 5.1.2 Diffusion model in Abaqus

The Figure 17 consists of a flowchart which describes the steps that were followed in Abaqus to build the model for diffusion analysis:

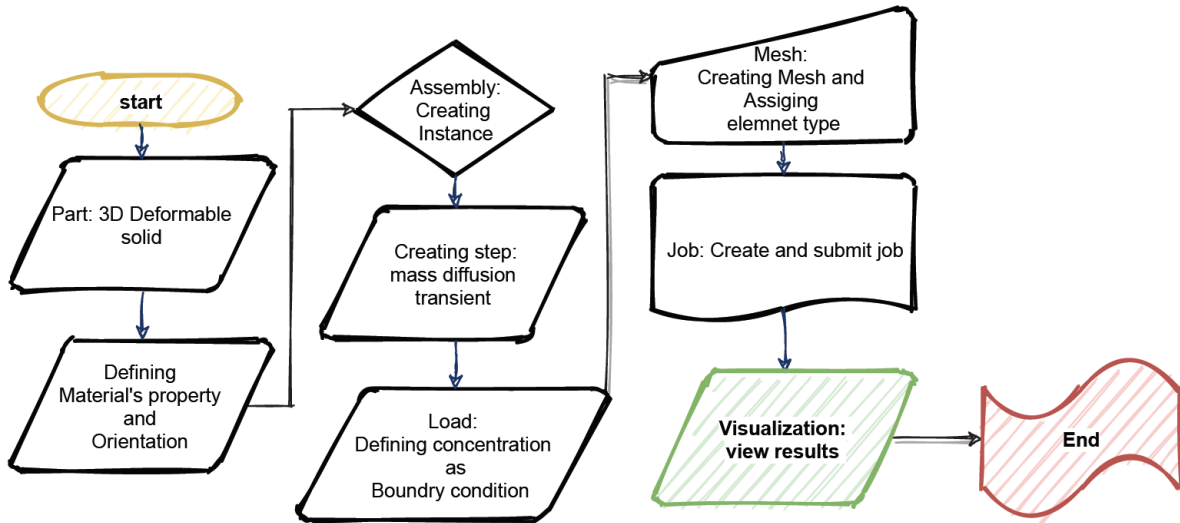


Figure 17: Abaqus Modelling process

Abaqus modelling was performed for the diffusion analysis to validate the optimized diffusion parameters obtained from the model created in Matlab. As it can be seen from the flow chart, the 3D deformable part was created in the shape and dimension mentioned in section 3.2.

#### 5.1.2.1 Material property

Defining the material’s property and fiber orientation was the next step. Three material behaviors were allocated including diffusivity, elastic, and solubility. The diffusivity was considered to be of an orthotropic nature and following the Fick’s law. Thus, the Table 5 consists of the diffusivity values used for the Abaqus model:

Table 5: Optimized Diffusivity values obtained from the Matlab Diffusion Model

D11	D22	D33	Concentration
0.01	0.004	0.0001	0

The concentration value was taken to be zero because it would signify that at the beginning of the experiment that the specimens have no oil particles present in their structure. Lastly, the D11, D22, and D33 values were taken from the Matlab model.

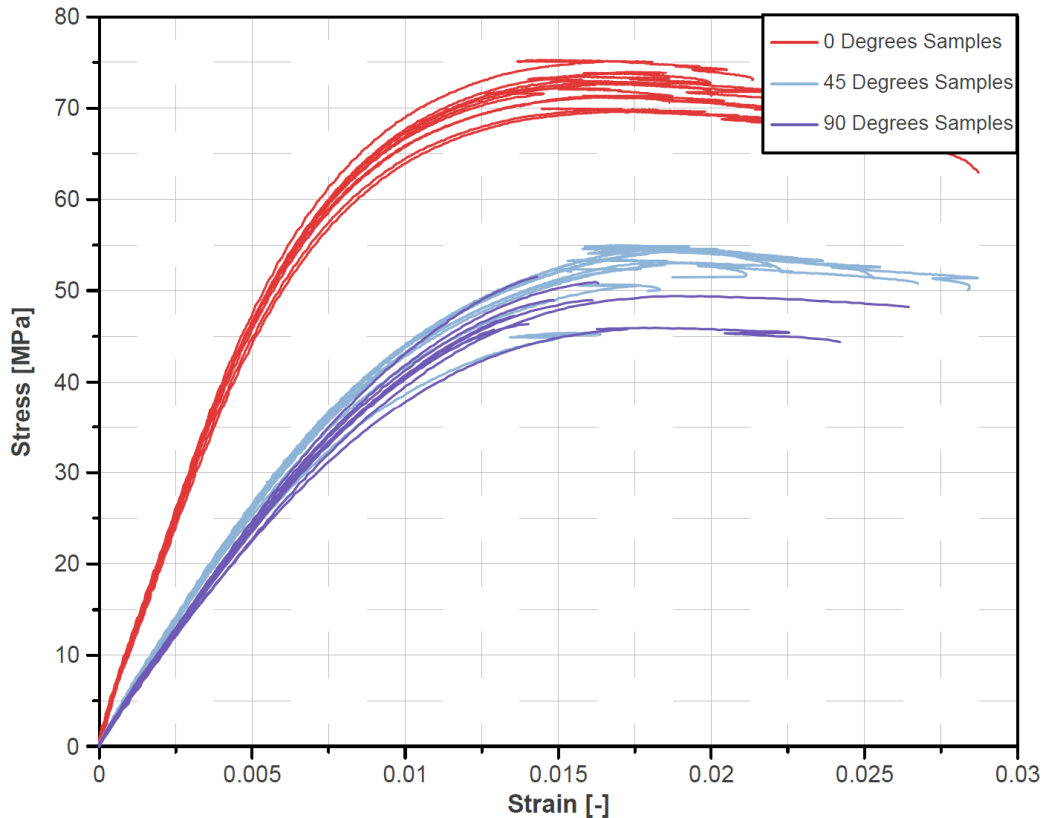


Figure 18: Stress-Strain curve of Dry specimens

The elastic properties of the specimen were obtained from the tensile testing of the dry specimens. As discussed in section 4.1, the raw tensile test data was processed in Diadem to obtain a stress and strain curve for each dry specimen. The Figure 18 consists of stress and strain curve of all the samples including 0-, 45-, and 90-degrees fiber orientation. It can be seen from the graph that the specimens with 0 degrees orientation withstood higher amount of stress before failing, while the 90 degrees fiber orientation specimens needed the least amount of stress to failure as compared to the other type of samples. In addition, the graph shows the average values of stress versus strain values across 10 samples for respective fiber orientation.

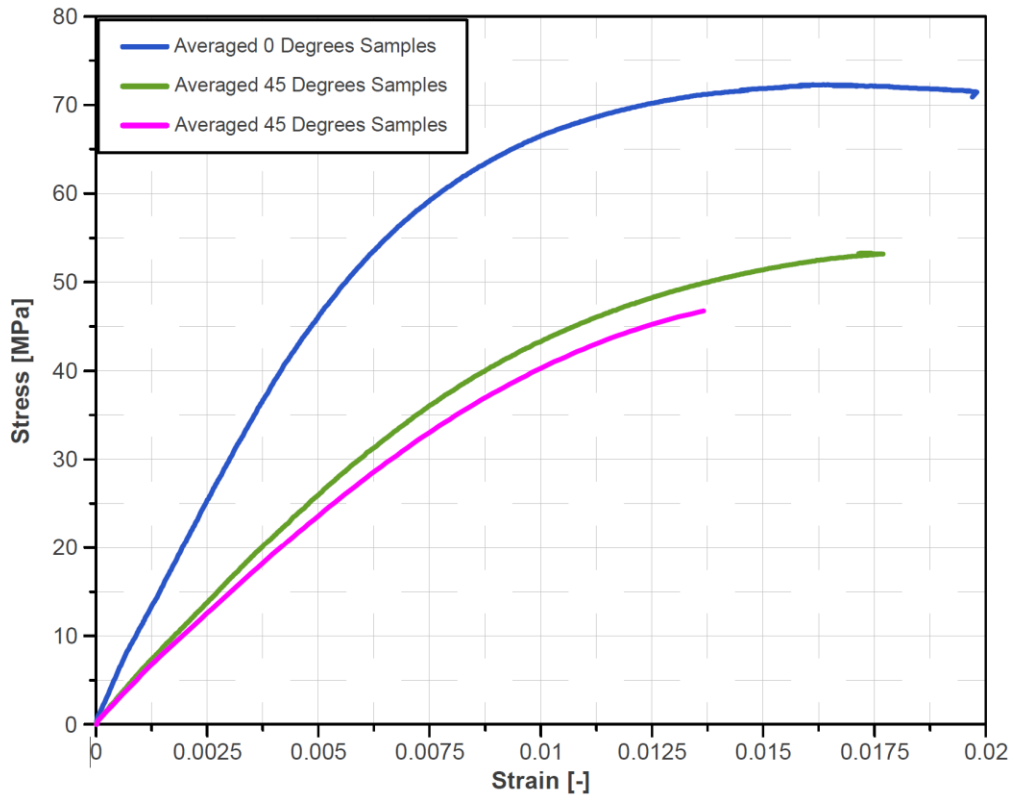


Figure 19: Average of Stress-Strain curve for each Orientation type (Dry specimens)

The Figure 19 consists of stress and strain data curve obtained from Diadem was used to compute materials properties of the dry samples which was used for the analysis in Abaqus. The Table 6 represents the Elastic properties assigned in the materials property section of the Abaqus model where E represents Young’s Modulus, Nu represents Poisson ratio, and G represents Shear Modulus:

Table 6: Elastic properties used for Diffusion model in Abaqus

<b>E1</b>	<b>E2</b>	<b>E3</b>	<b>Nu12</b>	<b>Nu13</b>	<b>Nu23</b>	<b>G12</b>	<b>G13</b>	<b>G23</b>
9.312 GPA	4.441 GPA	4.441 GPA	0.2521	0.3586	0.3586	5.5872 GPA	2.6643 GPA	2.6643 GPA

The solubility value for the diffusion model was taken as 1 which would signify that the concentration value obtained in the result section would be normalized concentration. Lastly,

these material's properties were assigned to the specimen by creating a section of the 3D part was solid and the assigned material properties are homogenous in nature.

The specimen's fiber orientation was defined in the material orientation section of the part geometry. In the material orientation panel, the orientation was defined discretely, and for the direction of fiber, angle of rotation of fiber was mentioned respectively for each sample type. The z axis or axis 3 was taken as normal axis as well as axis of rotation, and x-axis was primary axis. The Figure 20 shows the graphic representation of this process:

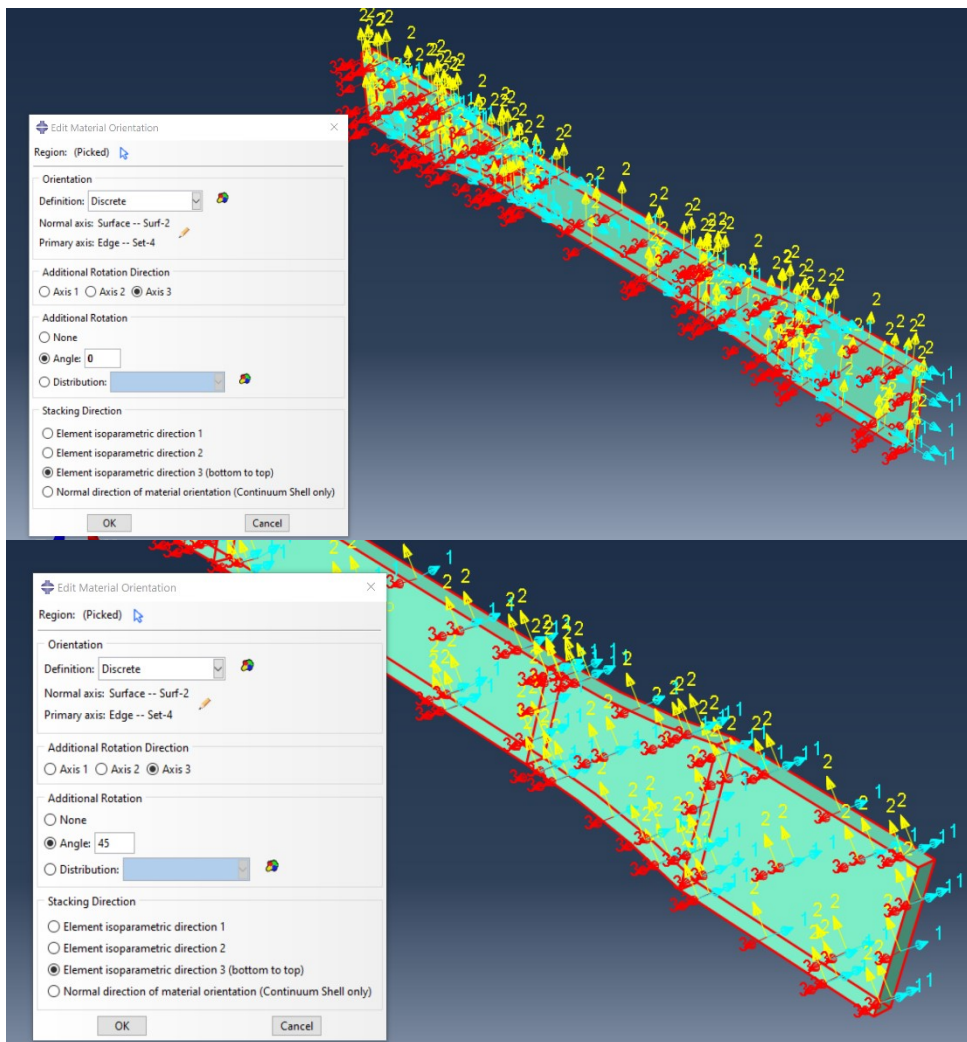


Figure 20: Defining the fiber orientation in Abaqus Modelling

### ***5.1.2.2 Assembly and step***

Once the material property was defined, an instance was created. An independent instance was created where the mesh will be created on the instance and not on the part itself. Thereafter, a in the step section, a mass diffusion step was created with a transient response and the time-period was selected to be 2966 which accounted for total number of hours under which the specimens were submerged in hot oil for the diffusion experiment. In addition, the incrementation type was taken to be fixed with increment size of 60. This incrementation size was selected considering that the specimens were taken out of oil tank once or twice a week to be weighed for obtaining mass-uptake data. Lastly, the maximum number of increments was taken to be 1000 for the analysis.

In addition to defining a step, it was also crucial to select the desired output parameters needed for the diffusion analysis once the job was been solved by the Abaqus. In Abaqus, there are two types of field output manager including F-Output manager and H-Output manager. For the analysis purpose, output variables such as concentration (CONC), normalized concentration (NNC), solute amount at each integration point (ISOL) were selected. Additionally, the output parameter such as amount of solute summed over a region (SOL) was selected from the H-Output manager. Consequently, the SOL was significant for the diffusion analysis and comparison of mass-uptake values obtained from experiment, Matlab, and Abaqus, however, NNC and CONC were used as an input parameter for the tensile test model in Abaqus which will be described in the section 5.2.

### ***5.1.2.3 Load***

As mentioned in the above sections of the report, the transport of oil particle was concentration driven, and Abaqus provides different options due to which the diffusion process could be influenced which includes pressure, concentration and/or temperature dependent. However, for the purpose of this study, it was sufficient to define the concentration value. This was performed

by defining boundary condition, where the relative value of concentration was defined to be 1 all the faces of the 3D-Part, as it can be seen in the Figure 21.

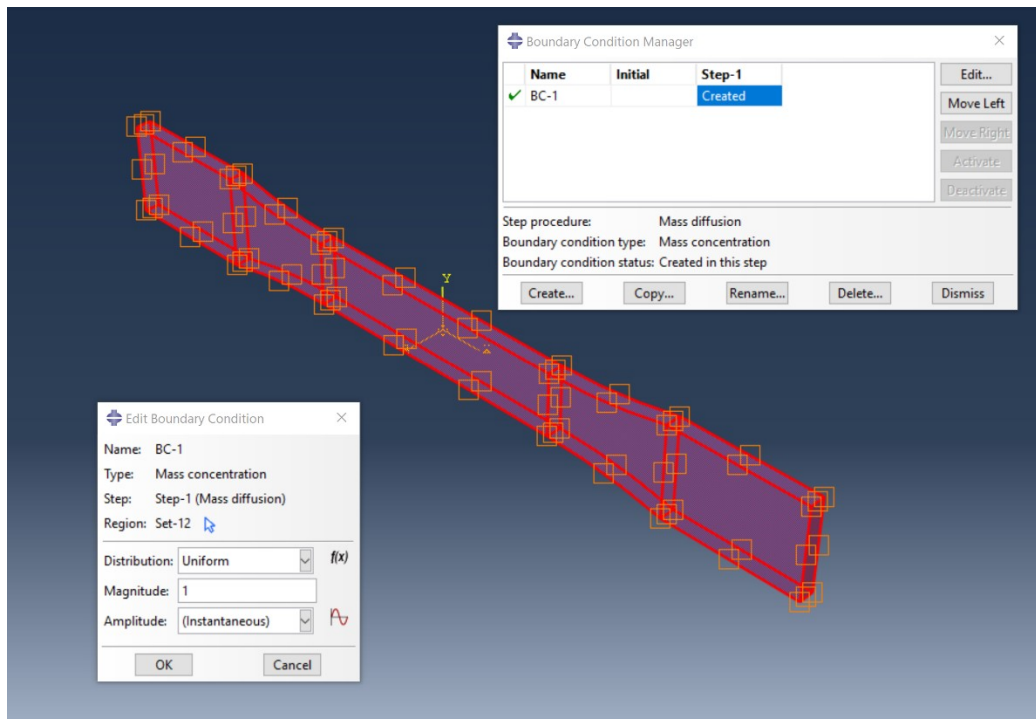


Figure 21: Defining the Boundary Conditions in Abaqus Model

#### 5.1.2.4 Mesh

To apply mesh to the part instance is one of the most crucial stages of the analysis. The quality of mesh will enhance the convergence process; hence, more accurate and precise results can be achieved. Also, it is the aim of the analysis which will define how fine the mesh should be, as the fine the mesh gets, the more computing time will be needed for the analysis. Specific to this study, the size control of the mesh was taken to be 1 for the global size with maximum deviation factor to be 0.1.

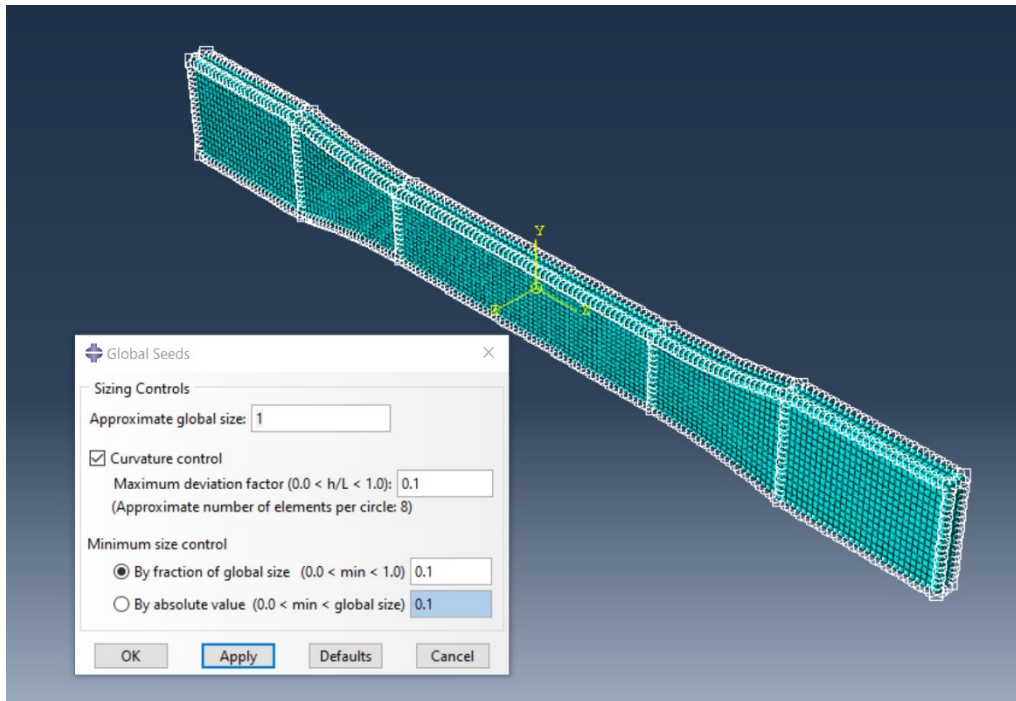


Figure 23: Mesh controls for diffusion model in Abaqus

The Figure 23 describes the meshing process graphically. The above mesh controls will yield 7968 number of elements for the 3D part instances. Lastly, it was crucial to define the type of elements

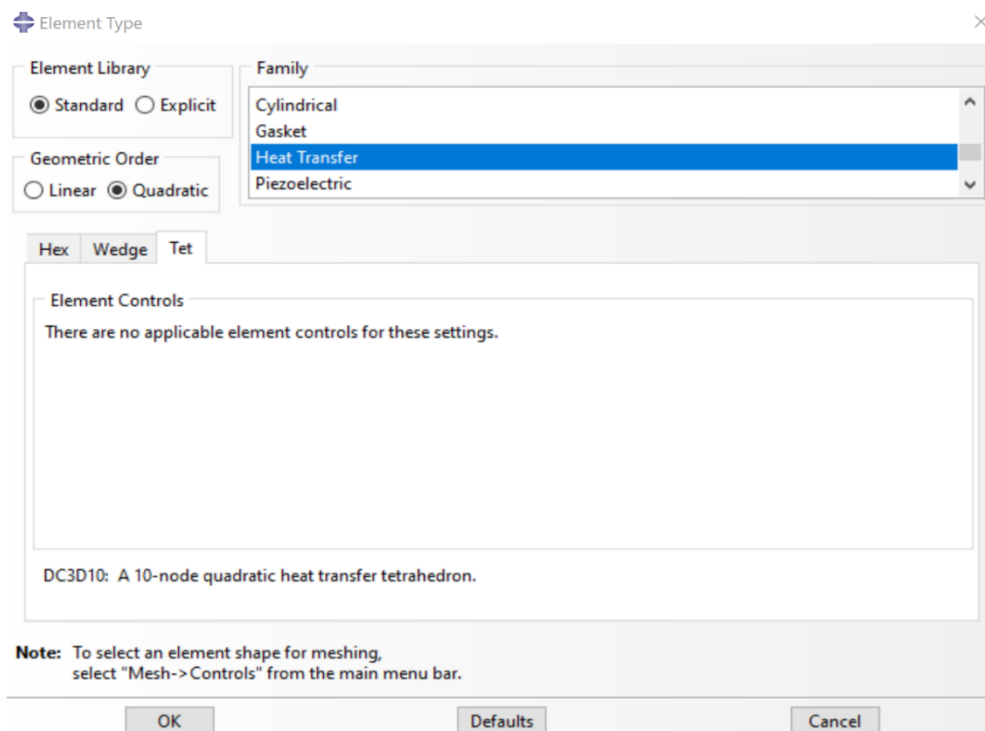


Figure 22: Element type selection for mesh elements

as selecting the wrong element type could yield inaccurate results, and the Figure 22 describes the element type selection using the element type wizard of Abaqus.

### 5.1.2.5 Job and Visualization

The final step of Abaqus modelling was to submit job and solve the diffusion problem. Once the results are obtained, the visualization section is used to obtain the XY data for the mass-up in relation to the time.

## 5.2 Determining sample degradation using Abaqus and experiment data for tensile testing

### 5.2.1 Material property

The material's property for tensile test modelling included defining Elastic and plastic properties. As mentioned in section 5.2.1.1 The elastic properties of the specimen were obtained from the tensile testing of the dry specimens and wet specimen. The raw tensile test data for the wet samples was processed in Diadem to obtain a stress and strain curve for each wet specimen.

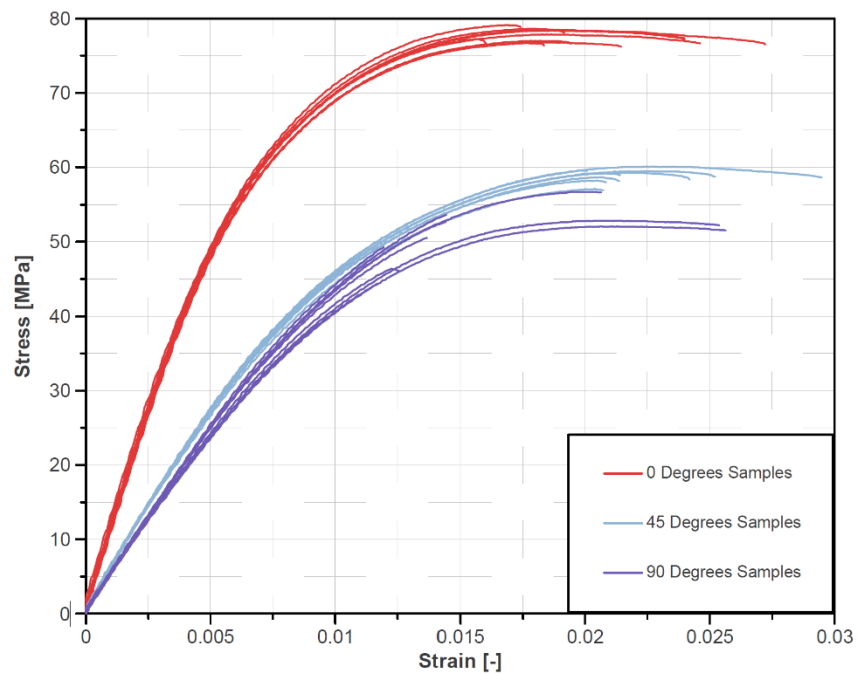


Figure 24: Stress-Strain curve for the wet specimens

The Figure 24 consists of stress and strain curve for the wet specimens for different fiber orientation. Like the data of dry specimens, it is evident from the graph that the specimens with 0 degrees orientation needed the maximum stress amount as compared to the 45 degrees and 90 degrees fiber orientation specimens. On the contrary, 90 degrees specimens needed the least amount of stress for it to fracture and fail.

The Figure 25 shows the average values of stress versus strain values across 10 samples for respective fiber orientation.

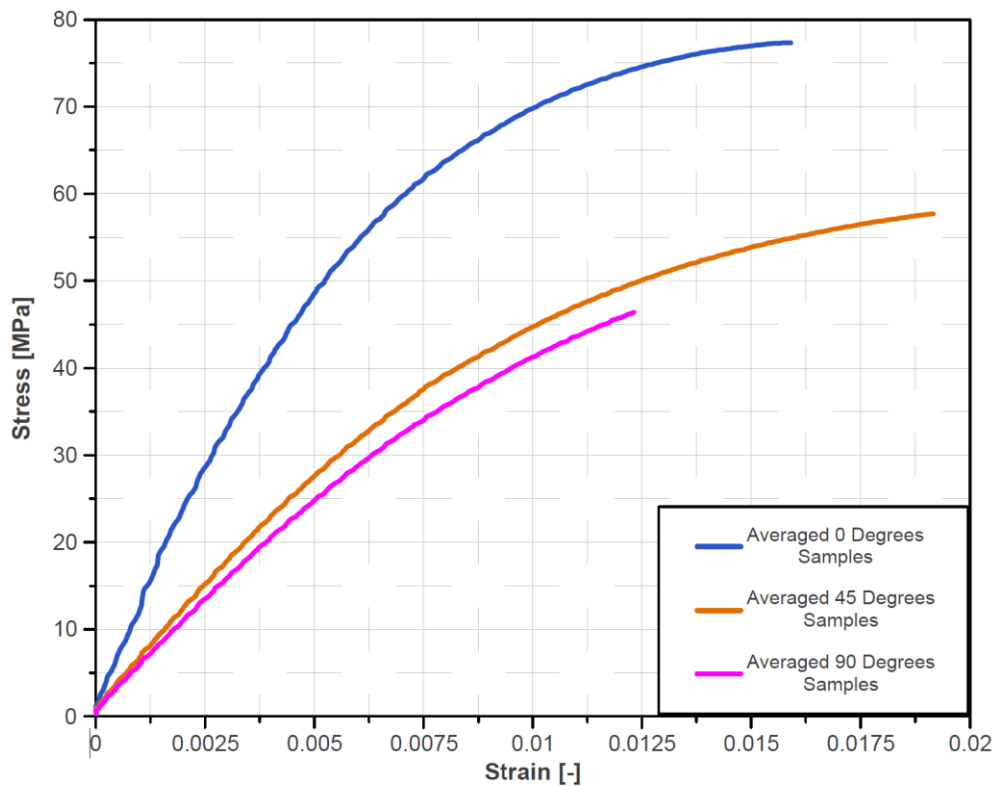


Figure 25: Average of Stress-Strain curve all the samples for each fiber orientations

The averaged stress and strain data was used to compute materials properties of the wet samples which was used for the degradation analysis in Abaqus. The Table 7 represents the Elastic properties assigned in the materials property section of the Abaqus model:

*Table 7: Elastic Properties for the Degradation model in Abaqus*

<b>E1</b>	<b>E2</b>	<b>E3</b>	<b>Nu1 2</b>	<b>Nu1 3</b>	<b>Nu2 3</b>	<b>G12</b>	<b>G13</b>	<b>G23</b>	<b>Fiel d 1</b>
9.312 GPA	4.441 <b>GPA</b>	4.441 <b>GPA</b>	0.25 21	0.35 86	0.35 86	5.5872 <b>GPA</b>	2.6643 <b>GPA</b>	2.6643 <b>GPA</b>	0
10.655 GPA	4.651 <b>GPA</b>	4.651 <b>GPA</b>	0.10 13	0.10 04	0.10 04	6.3927 <b>GPA</b>	2.7905 <b>GPA</b>	2.7905 <b>GPA</b>	1

### 5.2.2 Assembly and step

As mentioned in section 5.1.2.2, an independent instance was created. In addition, a step was created with time-period of 10, and with maximum number of increments to be 100 and an increment size of 0.1. These values were sufficient for the model to yield desired tensile test results.

In addition, F-Output field and H-Output field manager were used to select the desired output parameters for the model. Using the F-Output Field, output parameters consisted of Stress components, and invariants (S), Mises equivalent stress (MISES), Maximum Mises equivalent stress (MISESMAX), total strain components (E), Translations and rotations (U), total forces and moments (TF), and reaction forces and moments (RF). The H-Output field was used to obtain the output parameters including inertia relief load corresponding to equivalent rigid body acceleration (IRF), contact stresses (CSTRESS), total forces due to contact pressure (CFN), and critical stress at bond failure (CRSTS).

### 5.2.3 Interaction

A rigid body constraint was created between a user-defined reference point and one end of the specimen. The purpose of the constraint is to apply load at the reference point which is constrained with the end surfaces of the sample, thus, applying the force on reference point will apply pulling force on the specimen (Figure 26).

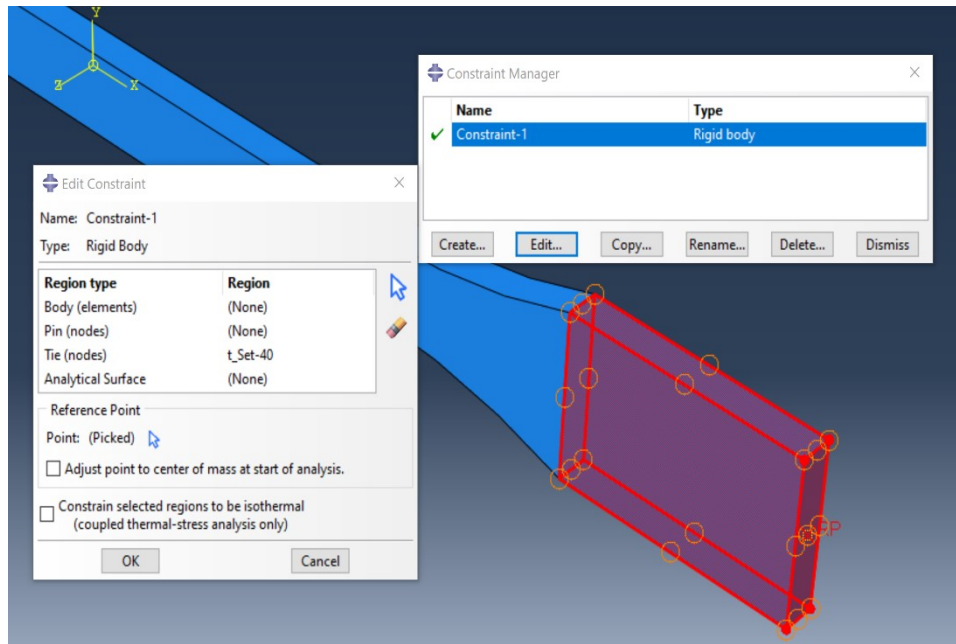


Figure 26: Constraint definition of rigid body type for the degradation model

### 5.2.4 Load

In the load section, the boundary conditions were assigned to the two opposite ends of the specimens. The one end of the specimens was defined to be fix in all planes (x, y, and z) meaning that there will be zero displacement and rotation in all direction. On the other hand, the opposite end of the specimen was only constrained in y and z direction and was free to move in the x

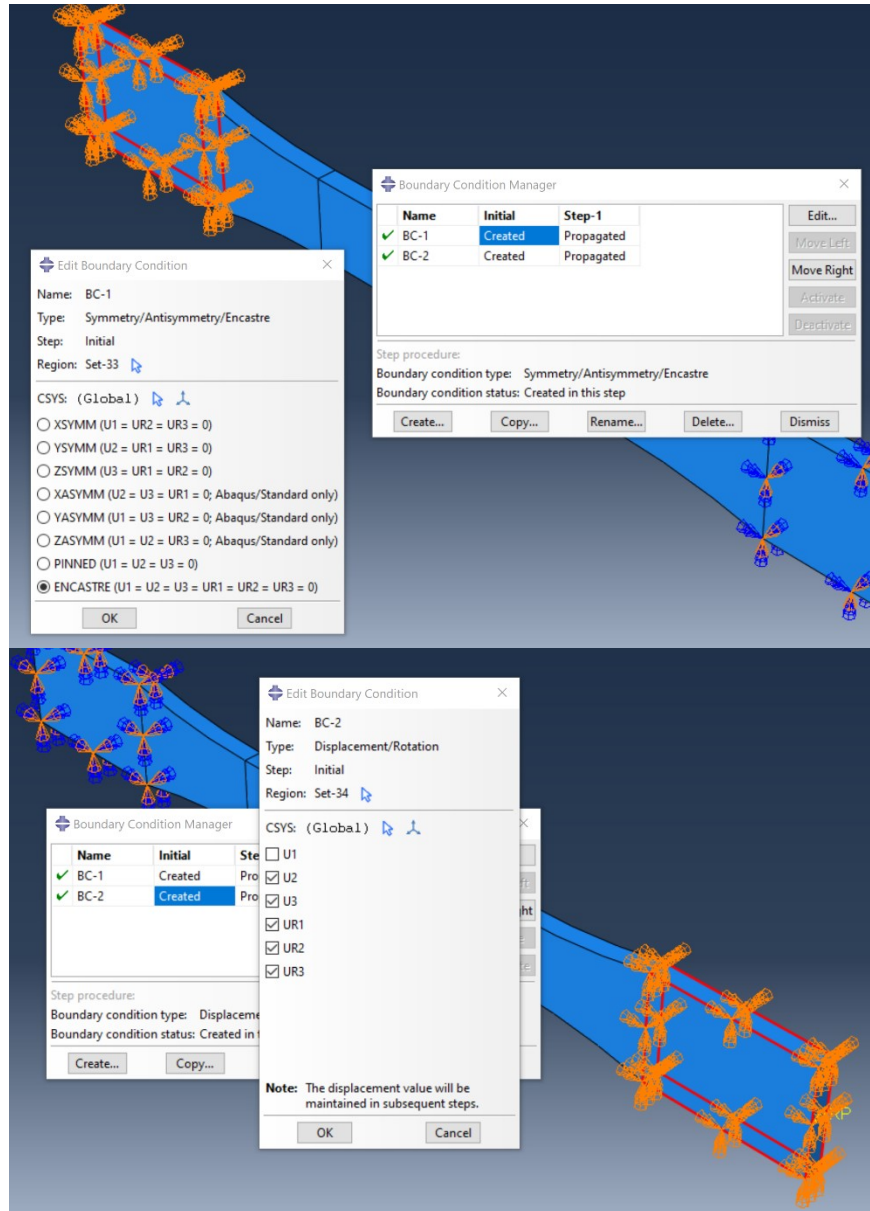


Figure 27: Definition of boundary condition for the degradation model

direction which is also the direction of pulling force being applied. The Figure 27 exemplifies the assignment of boundary conditions to the 3D composite part.

The Boundary Condition manager was also used to apply load at the one end of the specimen. The load was applied in the form of uni-axial displacement, and to achieve the specified value of displacement, Abaqus will assign a corresponding load is applied to the reference point (RP). The Figure 28 demonstrates how the uni-axial displacement was applied:

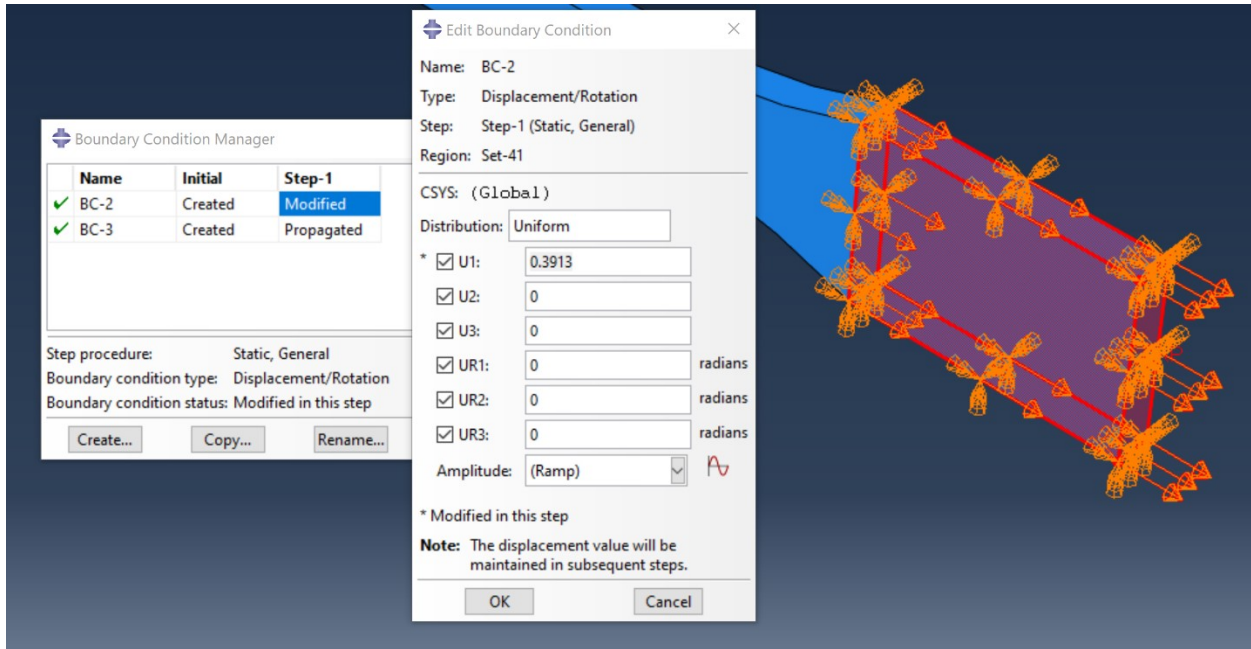


Figure 28: Applying the uni-axial Displacement at the one end of the dog-bone 3D part

Lastly, the predefined field manager was used to import the results of the diffusion model which would be used as an input parameter which would relate to the effect of oil diffusion in the specimen. Using the predefined field manager, diffusion model output file (.odb file) was uploaded to the current tensile test model. To be specific, the NNC out variable was used as an input which represents the normalized concentration of oil in the specimens. The Figure 29 demonstrates the definition of predefined field process:

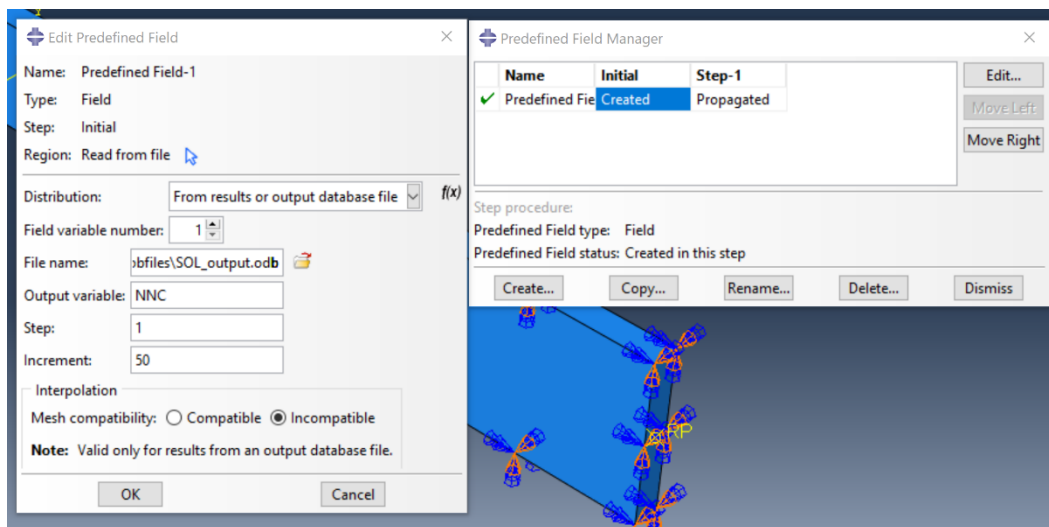


Figure 29: Assigning the pre-defined field for the degradation model

### 5.2.5 Mesh

As mentioned in the section 5.1.2.4, the quality of mesh will enhance the convergence process. In the mesh global seeds panel, the approximate global mesh size was taken to be 0.8. with minimum size control to be 0.1.

### 5.2.6 Job and Visualization

The final step of Abaqus modelling was to submit job and solve the diffusion problem. Once the results are obtained, the visualization section is used to obtain the XY data for the mass-up in relation to the time. The Figure 30 demonstrates the mesh on the 3D part instance:

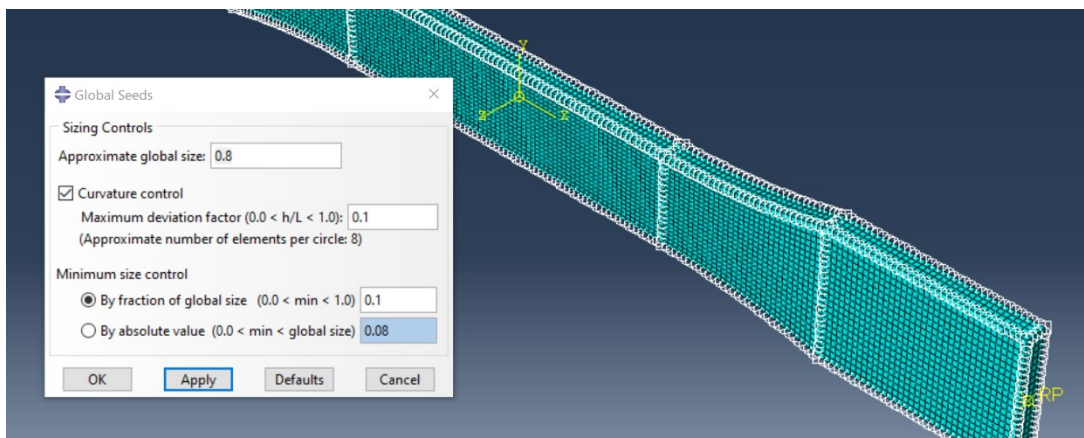


Figure 30: Mesh controls for the degradation model

The element type selected for the mesh elements was linear in nature and will be subjected to 3D stress. Lastly, the mesh process will create a total of 17388 elements.

## 6 RESULTS AND DISCUSSION

---

### 6.1 Diffusion model results

As mentioned in section 5 of this report, the optimized parameter obtained from the Matlab model were used to Abaqus diffusion model to validate the Matlab model, and to use the obtained normalized concentration results for the analysis of the tensile test modelling. The plots below describe the relative mass-uptake trend obtained from the experimental measurements, Matlab diffusion model, and Abaqus diffusion model.

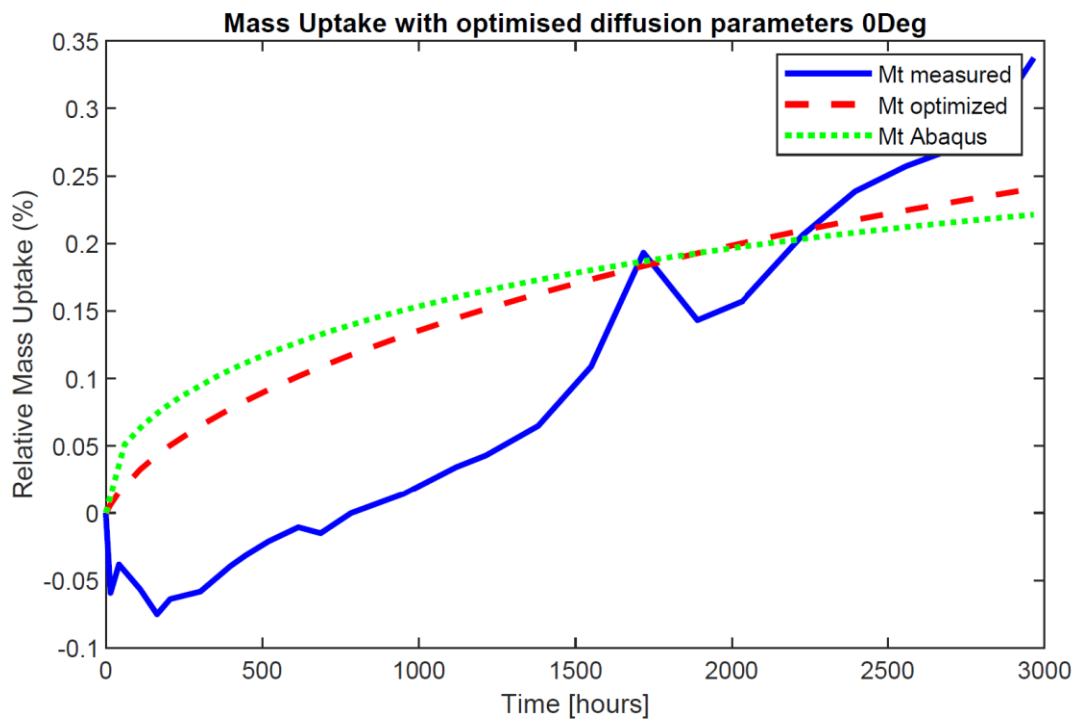


Figure 31: Mass-uptake for 0 Degree obtained from experiment, Matlab & Abaqus

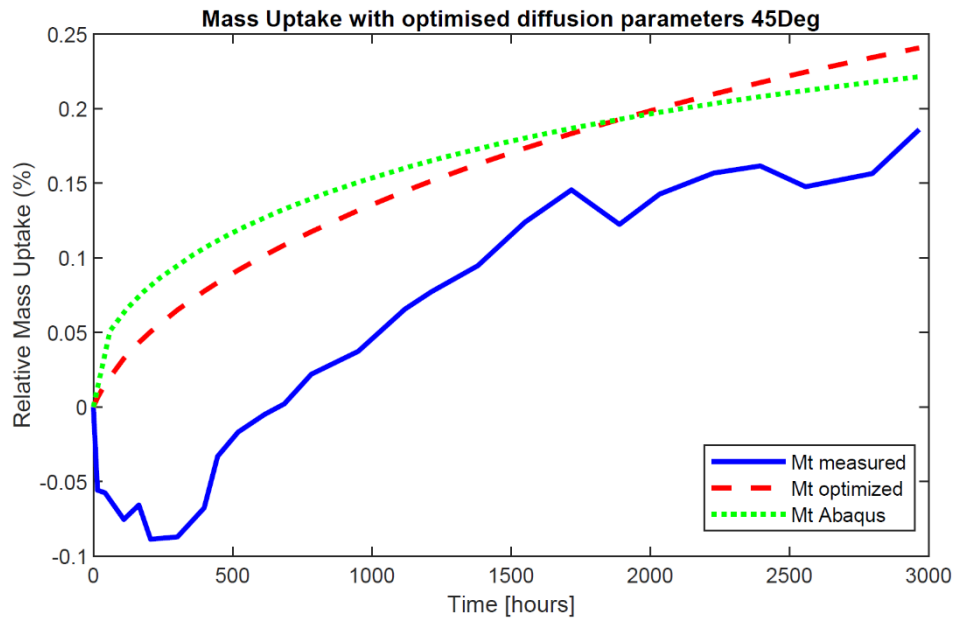


Figure 33: Mass-uptake for 45 Degree obtained from experiment, Matlab & Abaqus

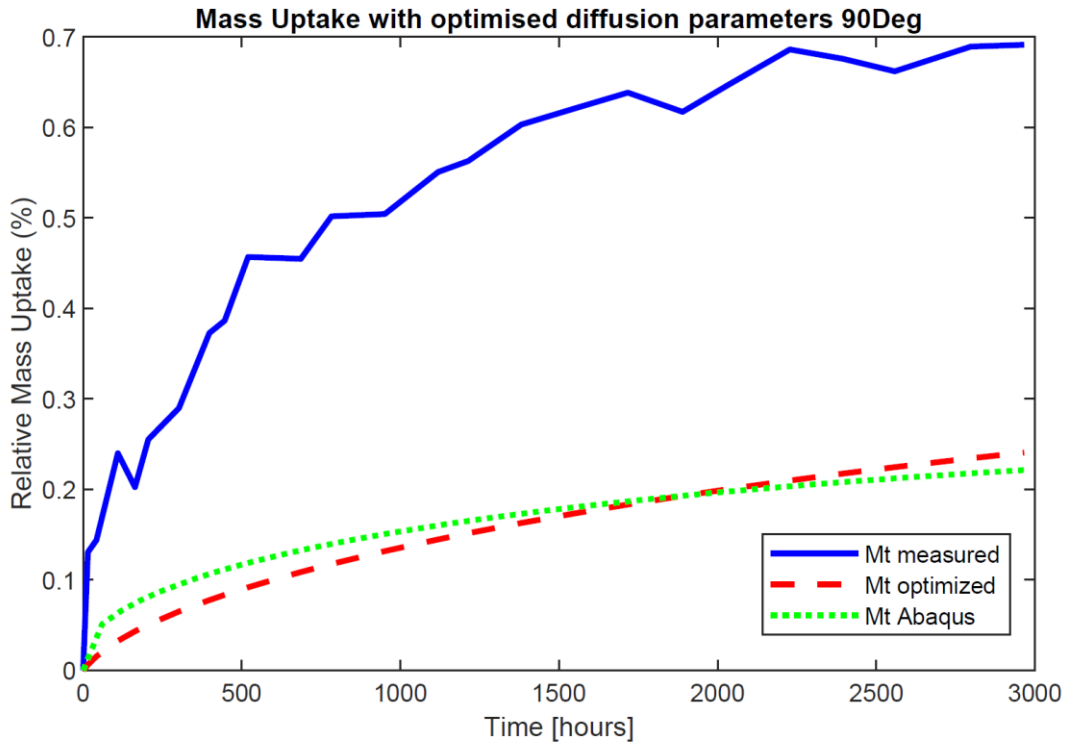


Figure 32: Mass-uptake for 90 Degree obtained from experiment, Matlab & Abaqus

The Figure 31, Figure 33, and Figure 32 represents the mass-uptake values for the 0-degree, 45-degree, and 90-degree fiber orientation respectively. As it can be seen from the figure that the Mass-uptake values obtained from the Matlab model followed the exponential trend whilst being as close as it can be to the real mass-uptake trend line obtained via experimentation. In addition, the results obtained from the Abaqus diffusion model were significantly similar and comparable to the results obtained from the Matlab model.

In the Figure 32, there is a big difference between the mass-uptake data obtained experimentally for 90-degree orientation samples and the Matlab model. These could possibly be due to the error function used for the objective function.

It is evident from the plot that the Abaqus diffusion model showed minor overestimation of mass-uptake data as compared to the data from the Matlab model. This could be due to the mesh size of the model in Abaqus needs to be smaller than what was considered. To solve the issue, mesh

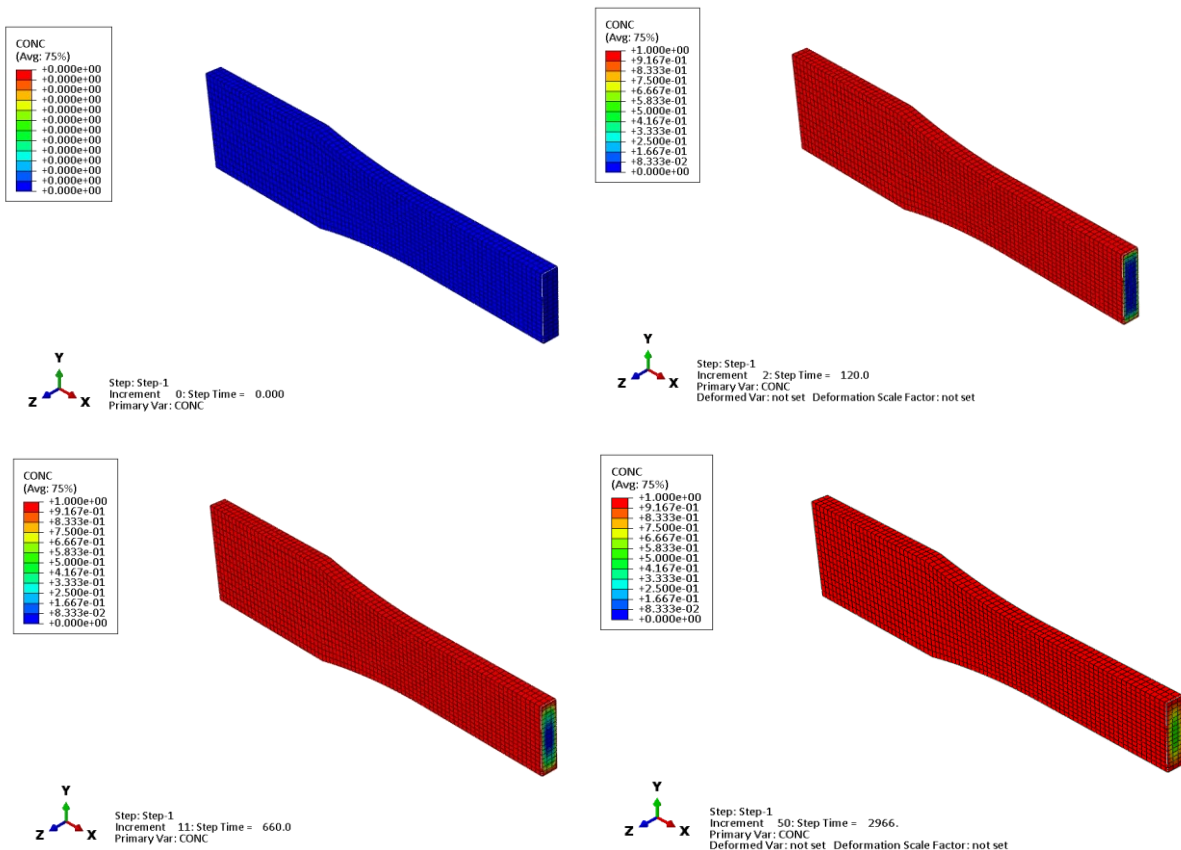


Figure 34: Diffusion results in Abaqus

convergence analysis can be performed, as it will enhance the accuracy and precision of obtained results.

The Figure 34 shows diffusion of oil into the 3D composite part in Abaqus. The figure demonstrates the diffusion process at 0 h, 120 h, 660 h, and 2966 h.

## 6.2 Tensile test results

### 6.2.1 Experimental tensile test results

As mentioned in section 4.1, the experimental data obtained from the tensile test experiment was processed in DIAdem to make comparison between preconditioned and post conditioned specimens to analyze their degradation due to the oil diffusion experiment. The comparison of

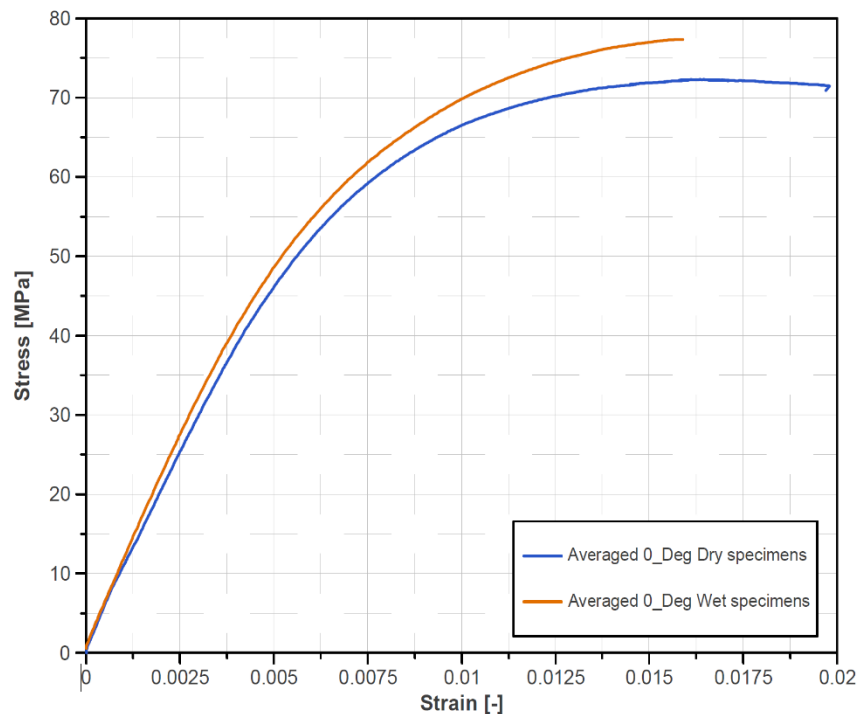


Figure 35: Experimental Stress-Strain curve for 0° specimen

stress strain curve obtained from the experimental was made to evaluate the level of degradation for each orientation type. The Figure 35, Figure 36 and Figure 37 which represents stress-strain relationship for 0°, 45° and 90° oriented specimens respectively. It is evident from the plots that

the specimen's toughness increased after they were exposed to oil for 2966 hours at constant temperature of 60°C. However, it was predicted that the specimens were supposed to degrade and possibly become weaker due to the diffusion of oil particles in the material. One of the possible explanations for such contradictory results could be that the annealing of the specimens could have happened due to longer exposure to elevated temperature which could have caused the material to become stronger. It is a typical manufacturing practice to perform annealing to minimize or redistribute the residual stress in the manufactured part, and the degree of crystallinity to be homogenized [28], which has a direct effect on stress-strain characteristic.

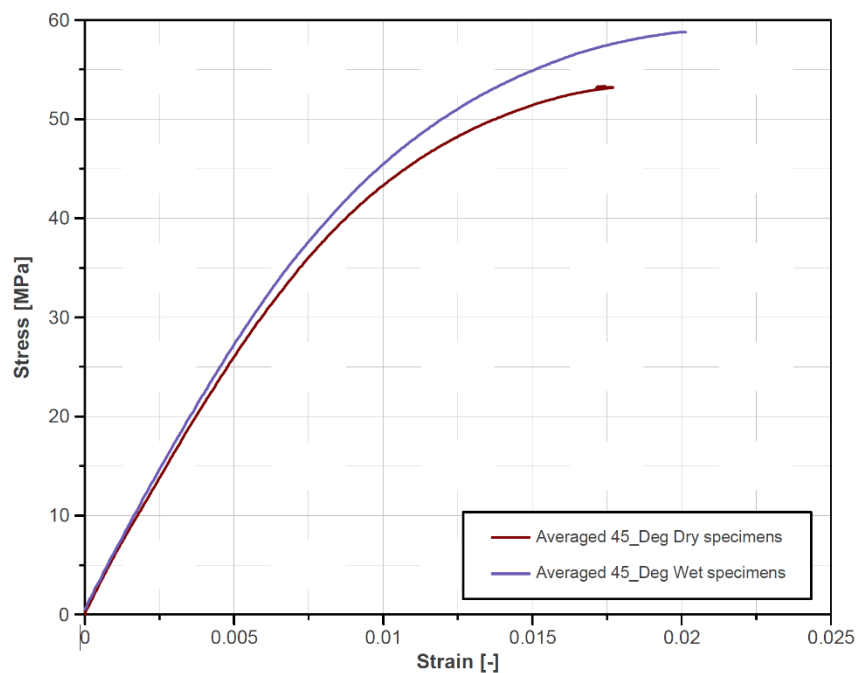


Figure 36: Experimental Stress-Strain curve for 45° specimen

Although the toughness increased for the specimen, maximum strain value for 0° and 90° had a slight decrease which could suggest that ductility of the specimens reduced post oil conditioning process. Nevertheless, it can be seen from the Figure 36 that the specimens with 45° fiber orientation saw a slight rise in both toughness and ductility. In addition, the maximum elongation for dry and wet specimens have been presented Figure 39. It can also be concluded that specimens with 0° fiber direction showed greater value of elongation as compared to 90° oriented specimens meaning specimens showed higher ductility when elongated along the fibers.

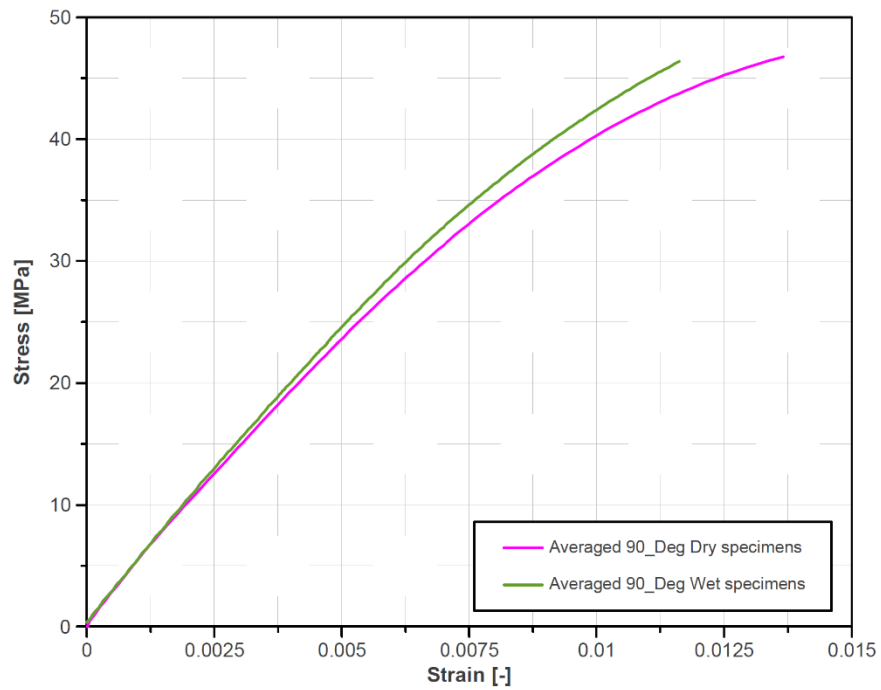


Figure 37: Experimental Stress-Strain curve for 90° specimen

From the stress-strain curve shown above, the materials properties such as Young's Modulus, Ultimate tensile strength, and maximum elongations were computed. It can be seen from the Figure 38 that the Young's modulus of wet specimens saw a slight increase from the values of the dry specimens. Specifically, there was significant rise for the specimens with 0° orientation from approximately 9 GPa to 10.5 GPa. Nonetheless, even though the young's modulus for 45° and 90° oriented specimen a minor increase post conditioning, the values remained comparatively similar to that of dry specimens, around 5 GPa and 4.5 GPa respectively.

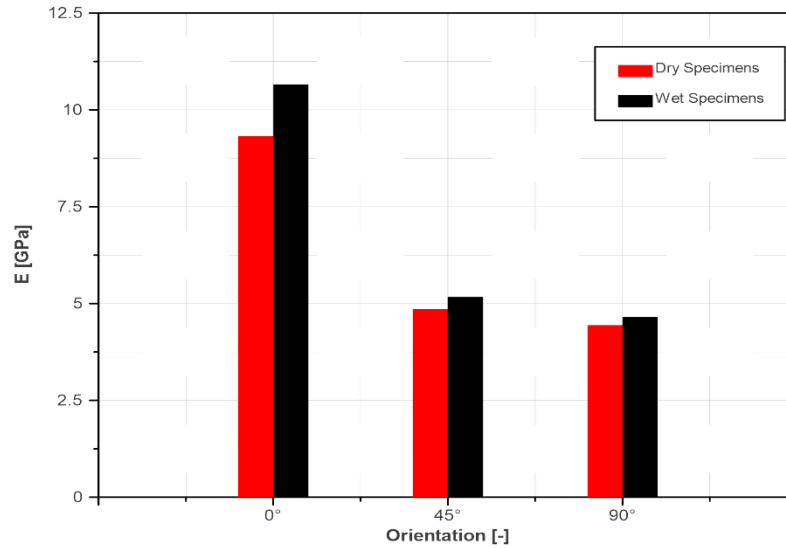


Figure 38: Experimental Young's modulus comparison between dry and wet specimens

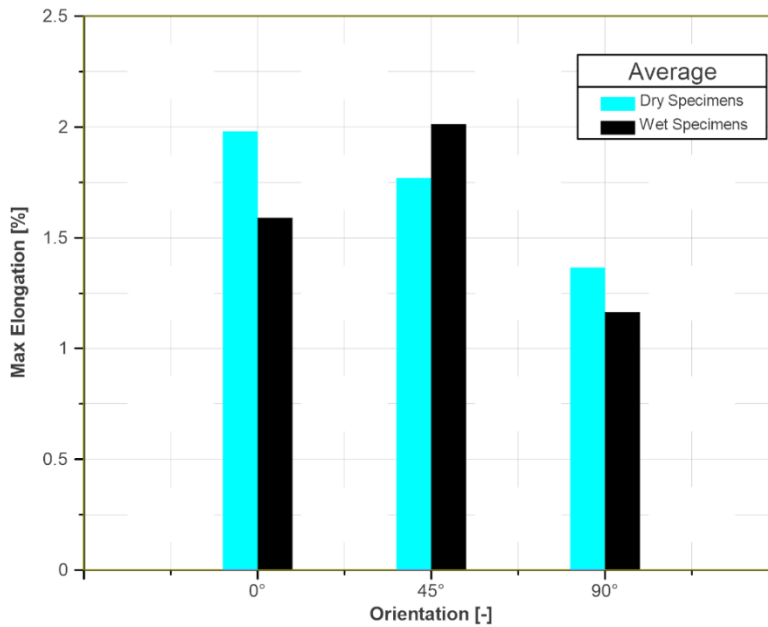


Figure 39: Max Elongation comparison between dry and wet specimens

Lastly, Figure 40 represents the ultimate tensile strength for the dry and wet specimens. It is evident from the figure that specimens could withstand higher values of load after being exposed to oil over a period. In addition, the figure also proves that specimens are the strongest when a load is applied in the longitudinal direction of the fiber orientation (0°-orientation), while the

specimen with transverse fiber orientation (90°-orientation) being subjected to a load in longitudinal direction are weakest.

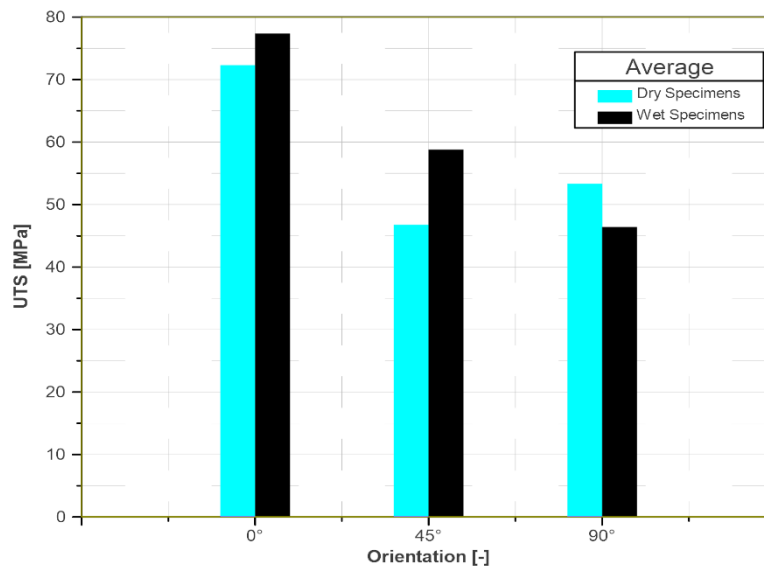


Figure 40: Ultimate Tensile Strength (UTS) comparison between dry and wet

### 6.2.2 Abaqus Tensile Test Result

The tensile test modelling in Abaqus was primarily performed to analyze the degradation effect on the elastic behavior of the conditioned specimen. For the purpose of analysis, the load versus displacement properties were obtained from the results of the tensile test model. Once the results were obtained from the FEM model in Abaqus, a comparison was made with the experimental data which included values for applied force and the corresponding displacement. The load and displacement data from the experiment and Abaqus model were plotted in a force versus displacement graph for different fiber orientation, and it can be found in Figure 41, Figure 42 and Figure 43.

It is evident from the Figure 42, Figure 41 and Figure 43 that the FEM model for tensile test analysis in Abaqus yielded similar value of displacement for respective longitudinal load applied on the composite specimen. For instance, in Figure 42, to achieve a displacement of 0.3913 mm, the experimental force noted was around 1495 N, and to achieve same displacement FEM model simulated a force of approximately 1569 N. Similarly, the experimental force values were comparatively similar to the simulated force for the same amount of displacement for the 45-

and 90-degree oriented samples. Thus, it can be said that the FEM model may have successfully modelled the experimental tests. In addition, the similarity of results from the FEM model of tensile test for the wet specimen validates the FEM model for the diffusion analysis performed in Matlab and Abaqus.

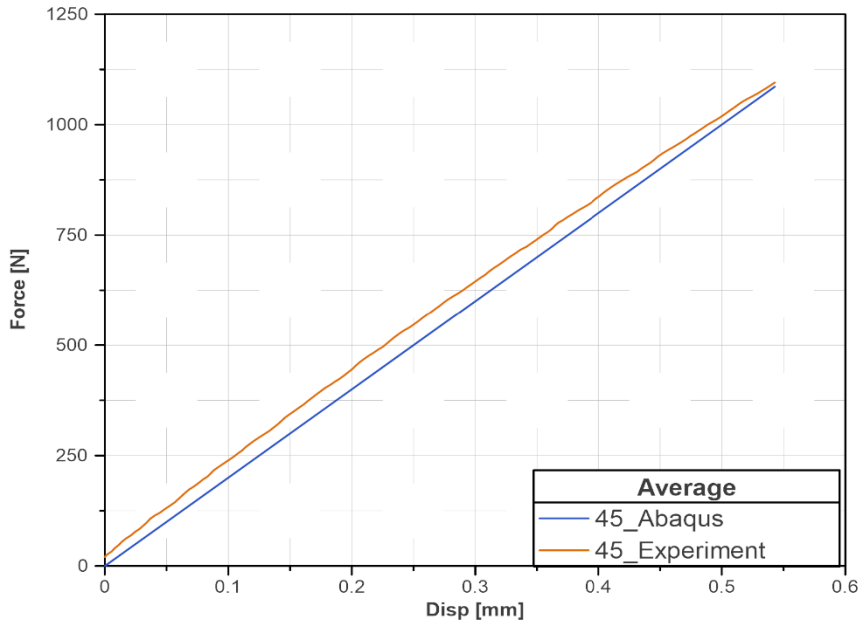


Figure 41: Load to Displacement comparison for 45° fiber-oriented specimens

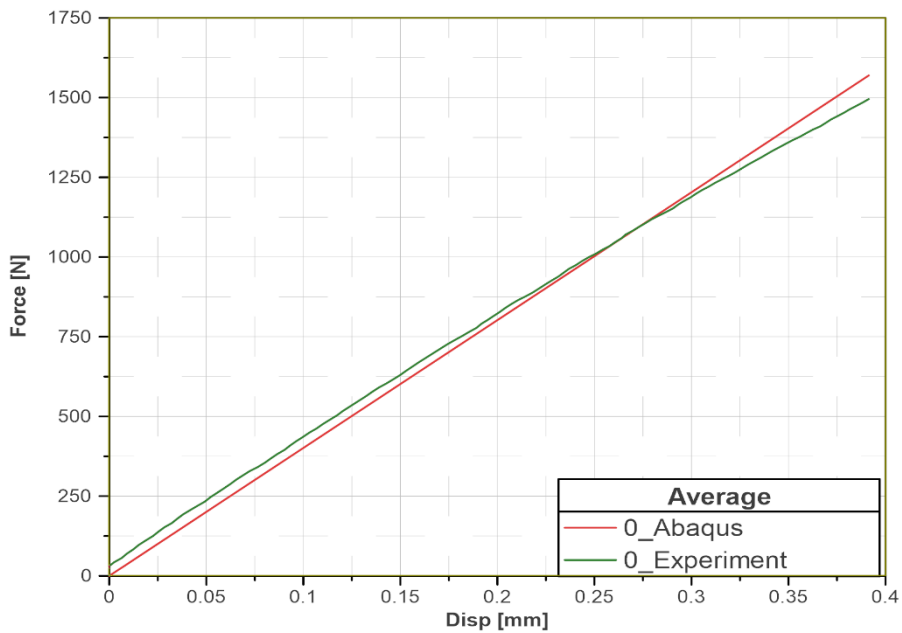


Figure 42: Load to Displacement comparison for 0° fiber-oriented specimens

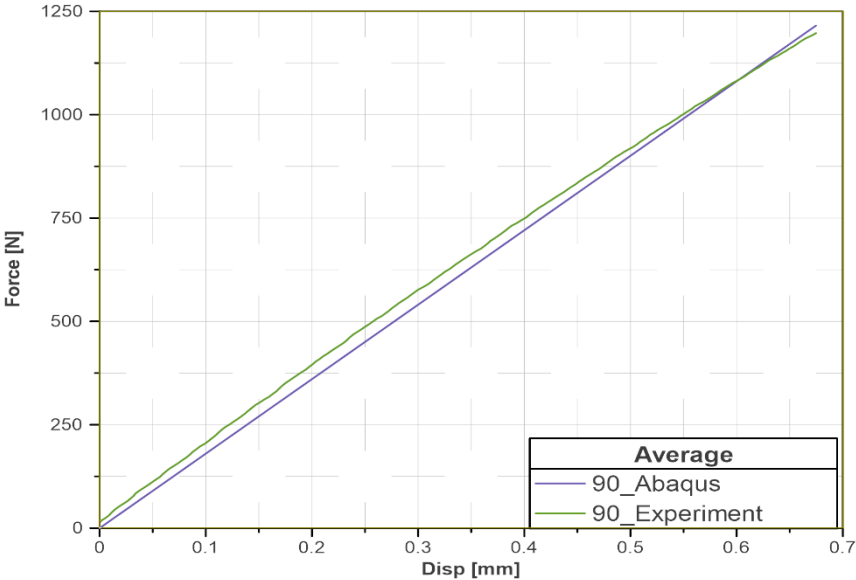


Figure 43: Load to Displacement comparison for 90° fiber-oriented specimens

However, it can be seen from the Figure 42, Figure 41 and Figure 43 that the accuracy and precision can be improved. Therefore, for the future analysis, the following presented in Table 8 recommendation can be made which could certainly enhance the analysis:

Table 8: Recommendations for future studies

<b>Recommendation for future studies</b>		
<b>Matlab Diffusion Model</b>	<b>Abaqus FEM Model for Diffusion Analysis</b>	<b>Abaqus FEM Model for Tensile test Analysis</b>
Need to have more accurate experimental data, by possibly using the composite laminates instead of 3D printed specimens	Mesh convergence analysis can be performed to achieve accurate and precise results	Mesh convergence analysis can be performed to achieve accurate and precise results
The error function needs to be revised to achieve more accurate and precise results		Analysis to address the plastic behavior of the composite specimens can be performed
Mesh convergence analysis can be performed for PDE FEM model to achieve accurate results		

## 7 CONCLUSION

---

This research project aimed to theoretically investigate the influence of working fluid such as oil on composite materials. In addition, building a FEM model for diffusion of fluid particle into the composite material and degradation of material due to working fluid absorption. Lastly, it was required to conduct experiment related to diffusion and tensile test through which data would be obtained which will be used for the constructed FEM model. Based on the diffusion analysis and tensile test analysis.

To address the requirements of the project, a comprehensive literature review was performed where influence of working fluid on composite material was studied. In addition, different possibilities of FEM modelling for diffusion of particles in composite materials was also researched. Based on the detailed literature review performed, experimental setup was constructed for the investigation of diffusion of oil into 3D printed composite samples. FEM model for diffusion analysis was built in Matlab which was validated using FEM model of diffusion in Abaqus. Lastly, to analyze the degradation of the oil in 3D printed composite samples, tensile test experiment was performed for dry and wet specimens, and its data was compared to the data of obtained from the FEM model of tensile test in Abaqus.

Based on the diffusion analysis of experimental data and FEM model data, it was found that the 3D printed specimens didn't accurately follow the Fickian law of diffusion where mass-uptake verses time curve in theory should follow an exponential upward trend for a diffusion process (refer Figure 15), and instead the experimental data saw an initial fluctuation in mass uptake values as shown in Figure 14. In addition, even though the FEM model could successfully model the diffusion of oil particle in composite specimens, and simulate the optimized value for diffusivities and solubility, the error function used for the optimization process in Matlab limited the model from yielding more accurate and precise diffusion parameters. Lastly, Abaqus FEM model of diffusion built in Abaqus successfully validated the Matlab model as the results of mass-uptake versus time plots very almost identical for both of the models.

Lastly, by performing the tensile test on dry and wet specimens, it was found that the wet specimens became stronger as their toughness increased after being exposed to hot oil for a period. In addition, the FEM model for tensile test in Abaqus successfully showed similar results for the load versus displacement data for the elastic behavior of the composite specimens which ultimately validated the FEM model.

To conclude, acknowledging the results obtained from the studies, the use of composite material in the automotive field will certainly keep increasing due to the obvious benefits of composite material parts over conventional metal parts. As the years pass by, more and more automotive parts will most likely be made of composite material. However, more research needs to be performed on the influence of working fluid on composite material.

## 8 BIBLIOGRAPHY

---

- [1] S. D. Mancini, A. d. O. S. Neto, M. O. H. Cioffi and E. C. Bianchi, "Replacement of metallic parts for polymer composite materials in motorcycle oil pumps," *Journal of Reinforced Plastics*, pp. 149-160, 2017.
  
- [2] Z. Huo, S. Anandan, M. Xu and K. Chandrashekhara, "Investigation of three-dimensional moisture diffusion modeling and mechanical degradation of carbon/bismaleimide composites under seawater conditioning," *Journal of Composite Materials*, vol. 52, no. 10, pp. 1339-1351, 2018.
  
- [3] University of Utah College of Engineering, "Research Report," University of Utah, Utah, USA, 2011.
  
- [4] J. H. S. A. Jr, S. D. B. Souza, E. C. Botelho and S. C. Amico, "Carbon fiber-reinforced epoxy filament-wound composite laminates exposed to hygrothermal conditioning," *Journal of Materials Science*, no. 51, p. 4697–4708, 2016.
  
- [5] A. Zhang, H. Lu and D. Zhang, "Synergistic effect of cyclic mechanical loading and moisture absorption on the bending fatigue performance of carbon/epoxy composites," *Journal of Materials Science volume*, vol. 49, pp. 314-320, 2014.
  
- [6] S. Mortazavian, A. Fatemi and A. Khosrovaneh, "Effect of Water Absorption on Tensile and Fatigue Behaviors of Two Short Glass Fiber Reinforced Thermoplastics," *SAE International Journal of Materials and Manufacturing*, vol. 8, no. 2, pp. 435-443, 2015.

- [7] X. S. Bian, L. Ambrosio, J. M. Kenny, L. Nicolais and A. T. Dibenedetto, "Effect of water absorption on the behavior of E-glass fiber/nylon-6 composites," *Polymer Composites*, vol. 12, no. 5, pp. 333-337, 1991.
- [8] X. Jiang, H. Kolstein, F. Bijlaard and X. Qiang, "Effects of hygrothermal aging on glass-fibre reinforced polymer laminates and adhesive of FRP composite bridge: Moisture diffusion characteristics," *Composites Part A: Applied Science and Manufacturing*, vol. 57, pp. 49-58, February 2014,.
- [9] H. Ishida and J. L. Koenig, "The reinforcement mechanism of fiber-glass reinforced plastics under wet conditions: A review," *Polymer Engineering and Science* , vol. 18, no. 2, pp. 128-145, February 1978.
- [10] S. B. Pillay, U. Vaidya and G. M. Janowski, "Effects of moisture and UV exposure on liquid molded carbon fabric reinforced nylon 6 composite laminates," *Composites Science and Technology*, vol. 69, no. 6, pp. 839-849, 2009.
- [11] Q. Zheng and R. Morgan, "Synergistic Thermal-Moisture Damage Mechanisms of Epoxies and Their Carbon Fiber Composites," *Journal of Composite Materials*, vol. 27, no. 15, pp. 1465-1478, 1993.
- [12] Z. A. M. Ishak and J. P. Berry, "Effect of moisture absorption on the dynamic mechanical properties of short carbon fiber reinforced nylon 6, 6," *Polymer Composites*, vol. 15, no. 3, pp. 223-230, 1994.
- [13] Y. Tsai, E. Bosze, E. Barjasteh and S. Nutt, "Influence of hygrothermal environment on thermal and mechanical properties of carbon fiber/fiberglass hybrid composites," *Composites Science and Technology*, vol. 69, pp. 432-437, 2009.

- [14] A. Zafar, F. Bertocco, J. Schjødt-Thomsen and J. Rauhe, "Investigation of the long term effects of moisture on carbon fibre and epoxy," *Composite Science and Technology*, vol. 72, pp. 656-666, 2012.
- [15] A. C. Loos and G. S. Springer, "Moisture Absorption of Graphite-Epoxy Composites Immersed in Liquids and in Humid Air," *Journal of Composite Materials*, vol. 13, no. 2, pp. 131-147, 1979.
- [16] P. Cherukupally, R. K. M. Chu, A. Bilton and C. B. Park, "Oil diffusion properties of acoustic foams for," in *AIP Conference Proceedings 1779*, 2016.
- [17] S. Jayakrishnan and G. Ragul, "EFFECT OF MECHANICAL PROPERTIES OF COMPOSITE MATERIAL UNDER THE INFLUENCE OF DIFFERENT COMMERCIAL OILS," *International Journal of Innovative Research in Technology*, vol. 2, no. 8, pp. 60-66, 2016.
- [18] Y. Fan, A. Gomez, S. Ferraro, B. Pinto, A. Muliana and V. L. Saponara, "Diffusion of water in glass fiber reinforced polymer composites at different temperatures," *Journal of Composite materials*, vol. 53, no. 8, pp. 1097-1110, 2018.
- [19] A. Gagani, Y. Fan, A. H. Muliana and A. T. Echtermeyer, "Micromechanical modeling of anisotropic water diffusion in glass fiber epoxy reinforced composites," *Journal of Composite Materials*, vol. 52, no. 17, pp. 2321-2335, 2017.
- [20] G. He and Y. Liu, "Theoretical Modeling of the Mechanical Degradation of Polymer Composites due to Moisture/Water Absorption and Damage Progression," *SAE Technical Paper*, 2019.

- [21] COLORFABB, "Technical datasheet," colorFabb, 6 April 2020. [Online]. Available: <https://colorfabb.com/xt-cf20>. [Accessed 2020].
- [22] Parmo, "MOGUL CLP 100/10," Parmo, 4 April 2020. [Online]. Available: <https://eshop.paramo.cz/zbozi.aspx?kod=V032158310>. [Accessed 2020].
- [23] The MathWorks, Inc., "fmincon," 2020. [Online]. Available: <https://www.mathworks.com/help/optim/ug/fmincon.html>.
- [24] J. Crank, *The Mathematics of Diffusion*, London: Oxford, 1975.
- [25] E. J. Barbero, *Finite element analysis of composite materials*, CRC press, 2008.
- [26] Dassault Systems, "Abaqus Analysis User's Manual," 13 February 2012. [Online]. Available: <http://dsk-016-1.fsid.cvut.cz:2080/v6.12/books/usb/default.htm?startat=pt03ch06s09at28.html#usb-anl-amassdiffusion>. [Accessed 2020].
- [27] The MathWorks, Inc, "General PDEs," 2021. [Online]. Available: <https://au.mathworks.com/help/pde/>.
- [28] T. Tsukada, S. Minakuchi and N. Takeda, "Assessing residual stress redistribution during annealing in thick thermoplastic composites using optical fiber sensors," *The Journal of Thermoplastic Composite Materials*, vol. 33, no. 1, pp. 53-68, 2018.

[29 C. J, *The Mathematics of Diffusion*, London: Oxford, 1975.

[30 T. deV.Naylor, "Permeation Properties," in *Comprehensive Polymer Science and Supplements*, Sunbury-on-Thames, The British Petroleum Company plc, 1989, pp. 643-668.